

A mathematical model for tumor–immune dynamics in multiple myeloma

Jill Gallaher, Kamila Larripa, Urszula Ledzewicz, Marissa Renardy, Blerta Shtylla, Nessay Tania, Diana White, Karen Wood, Li Zhu, Chaitali Passey, Michael Robbins, Natalie Bezman, Suresh Shelat, Hearn Jay Cho*, Helen Moore*†

* Contributed equally to the building of the model and the conceptual framework.

† Corresponding author.

Jill Gallaher

H. Lee Moffitt Cancer Center, Tampa, FL 33612, e-mail: jill.gallaher@moffitt.org

Kamila Larripa

Department of Mathematics, Humboldt State University, Arcata, CA 95521, e-mail: kamila.larripa@humboldt.edu

Urszula Ledzewicz

Department of Mathematics and Statistics, Southern Illinois University Edwardsville, Edwardsville, IL 62026 and Institute of Mathematics, Lodz University of Technology, 90-924 Lodz, Poland, e-mail: uledzew@siue.edu

Marissa Renardy

Department of Mathematics, The Ohio State University, Columbus, OH 43210,

Current address: Department of Microbiology and Immunology, University of Michigan, Ann Arbor, MI 48109, e-mail: renardy@umich.edu

Blerta Shtylla

Mathematics Department, Pomona College, Claremont, CA 91711, e-mail: shtyllab@pomona.edu

Nessay Tania

Department of Mathematics and Statistics, Smith College, Northampton, MA 01063, e-mail: ntania@smith.edu

Diana White

Department of Mathematics, Clarkson University, Potsdam, NY 13699, e-mail: dtwhite@clarkson.edu

Karen Wood

Department of Mathematics, University of California at Irvine, Irvine, CA 92697,

Current address: The Aerospace Corporation, El Segundo, CA 90245, e-mail: kewood@uci.edu

Li Zhu

Clinical Pharmacology and Pharmacometrics, Bristol-Myers Squibb, Princeton, NJ 08543, e-mail: li.zhu@bms.com

Chaitali Passey

Clinical Pharmacology and Pharmacometrics, Bristol-Myers Squibb, Princeton, NJ 08543, e-mail: chaitali.passey@bms.com

Michael Robbins

Hematology Medical Strategy, Bristol-Myers Squibb, Lawrence Township, NJ 08648, e-mail: michael.robbins@bms.com

Natalie Bezman

Immuno-Oncology Discovery, Bristol-Myers Squibb, Redwood City, CA 94063, e-mail:

Abstract We propose a mathematical model that describes the dynamics of multiple myeloma and three distinct populations of the innate and adaptive immune system: cytotoxic T cells, natural killer cells, and regulatory T cells. The model includes significant biologically- and therapeutically-relevant pathways for inhibitory and stimulatory interactions between these populations. Due to the model complexity, we propose a reduced version that captures the principal biological aspects for advanced disease, while still including potential targets for therapeutic interventions. Analysis of the reduced two-dimensional model revealed details about long-term model behavior. In particular, theoretical results describing equilibria and their associated stability are described in detail. Consistent with the theoretical analysis, numerical results reveal parameter regions for which bistability exists. The two stable states in these cases may correspond to long-term disease control or a higher level of disease burden. This initial analysis of the dynamical system provides a foundation for later work, which will consider combination therapies, their expected outcomes, and optimization of regimens.

1 Introduction

Multiple myeloma (MM) is a cancer of plasma cells, and is diagnosed in approximately 30,000 patients in the United States annually [80]. Current standard therapies include combinations of proteasome inhibitors, immunomodulatory drugs, glucocorticoids, and high dose chemotherapy and autologous stem cell rescue. Recent approvals for targeted monoclonal antibodies, including daratumumab and elotuzumab, have resulted in substantial improvements in survival, but few patients survive more than ten years [43]. There have been attempts to control the disease using immune modulation; however, outstanding questions remain unanswered regarding both treatment choice and timing [43, 46]. Drugs are commonly used in combination, and with the number of available therapies and the complex feedback between the tumor and immune system, finding the best combinations of treatments for different stages is a challenge.

natalie.bezman@bms.com

Suresh Shelat

Oncology Clinical Development, Bristol-Myers Squibb, Lawrence Township, NJ 08648, e-mail: suresh.shelat@bms.com

Hearn Jay Cho

Tisch Cancer Institute, Mt. Sinai School of Medicine, New York, NY 10029, e-mail: hearn.jay.cho@mssm.edu

Helen Moore

Quantitative Clinical Pharmacology, Bristol-Myers Squibb, Princeton, NJ 08543

Current address: Drug Metabolism and Pharmacokinetics, AstraZeneca, Waltham, MA 02451, e-mail: dr.helen.moore@gmail.com

In this work, we present a “within-host” mathematical model of MM (“tumor”) and immune system dynamics that can be used for exploring combination therapy effects *in silico*. Our model tracks tumor burden in a hypothetical patient with MM and several immune cell types that play important roles in disease control or progression. We include key model components and interactions between them to reflect the biology and to represent targets for therapeutic intervention. We explain the significant components of the model, establish how these components influence each other, and explore some of the underlying properties of the model with regard to conditions for disease stability and control. The goal of this work is to determine and justify the model, and to explore its basic properties. In the future, we plan to use this foundation to explore and optimize treatment regimens for patients with MM in various settings.

There is a rich history of mathematical models for tumor-immune system interactions. One of the first papers in which such a model was formulated is that of Stepanova [84] in 1980. The model highlighted the strong nonlinear interplay and underlying kinetics between a tumor and an aggregate immune system and resulted in multi-stability. This model is the basis for numerous extensions and generalizations such as models by Kuznetsov et al. [48], Kirschner and Panetta [45], de Vladar and González [19], d’Onofrio [24], and de Pillis et al. [18]. These models are formulated and analyzed as dynamical systems described by ordinary differential equations (ODEs) while other modeling approaches include structured population models [20], partial differential equations (PDEs) [55], cellular automata models [91], or combinations of these approaches [12]. Additional modeling approaches for tumor-immune system interactions can be found in Eladaddi et al. [27] and Schättler and Ledzewicz [75]. While many of these models consist of very general descriptions of cancer dynamics, other papers analyze tumor-immune system interactions for specific cancer types. Examples of such models include papers by Moore et al. on chronic myeloid leukemia [52, 61, 62].

In this work, we model population dynamics in the peripheral blood of patients with MM, although much of these dynamics are driven by interactions that occur elsewhere (e.g., in the bone marrow or lymph nodes). Levels of myeloma protein (M protein) in peripheral blood samples are correlated with tumor burden [74]. This protein is typically a monoclonal immunoglobulin or a monoclonal free light chain produced by the malignant plasma cells and has harmful effects, such as increased blood viscosity and organ damage [56]. Sullivan and Salmon [86] developed a simple tumor growth mathematical model in the early 1970s using M-protein levels to study chemotherapy-induced tumor regression in patients with MM. Optimal control principles were shortly thereafter applied in Swan and Vincent [88] to show an optimal dosing strategy for patients with MM under chemotherapy.

In 2016, Tang et al. [89] published a model fit to data from three bortezomib-based chemotherapy clinical trial cohorts of patients with MM. Their mathematical model proposed a differentiation hierarchy in the bone marrow with a myeloma progenitor cell population that was relatively resistant to therapy. They showed that rationally-designed combination treatments with decreased selection pressure on myeloma cells can lead to a longer remission period.

Overall, prior studies have shown that mathematical modeling in the context of MM can be a valuable tool with the potential to improve treatments. However, these prior studies have not examined the role of the immune system in MM disease dynamics. Several immunomodulatory drugs have been approved for use in MM, and more are in the pipeline. As we plan to eventually optimize regimens for patients with MM and include immunotherapies, in this work we develop and analyze a mathematical model that captures key tumor–immune interactions in patients with MM.

The mathematical model we propose consists of a dynamical system that tracks a tumor burden marker and several immune cell components. We track the level of M protein in the peripheral blood, which is commonly used as a key diagnostic indicator and as a surrogate of tumor burden in patients with MM [26]. The immune cells included in our model are cytotoxic T lymphocytes, natural killer cells, and regulatory T cells. We perform equilibrium and stability analysis to determine the conditions under which stable disease “immune-controlled” states exist. In particular, we explore regions of parameter space for which a long-term disease control (LTDC) state exists (represented by a lower stable equilibrium value for M protein), and for which a stable state of high tumor burden exists. In addition, we numerically simulate certain disease conditions to better understand how the system evolves. This initial analysis of the dynamical system provides a foundation for later work, in which we will consider combination therapies, their expected outcomes, and optimization of regimens.

2 Mathematical Model

Our mathematical model consists of a system of ordinary differential equations that describes interactions between MM and the immune system. Specifically, we track the temporal dynamics of the following four populations in the peripheral blood: M protein produced by MM cells, $M(t)$; cytotoxic T lymphocytes (CTLs), $T_C(t)$; natural killer (NK) cells, $N(t)$; and regulatory T cells (Tregs), $T_R(t)$. The NK population is part of the innate immune system, while CTL and Tregs are part of the adaptive immune response and are assumed to be specific to myeloma cells. The three immune cell populations included in the model were also chosen for the following additional reasons. First, they are all implicated in the development of MM [25, 41], and have interrelated dynamics [25]. Second, each is affected by a therapy we plan to study *in silico* with this model: NK cells are targeted by the approved MM therapy elotuzumab [67]; Tregs are affected by the approved MM therapy daratumumab [47]; and the main effect of anti-programmed death 1 (anti-PD-1) therapy is on effector T cells [66]. Third, levels of each of the three immune cell types could be obtained from patient peripheral blood samples in clinical studies, which would allow the estimation of certain parameters in the model. The interactions between populations included in this model are illustrated in Fig. 1 and listed in Table 1.

In Section 2.1, we discuss in greater detail the biological basis for each interaction pathway used in the model.

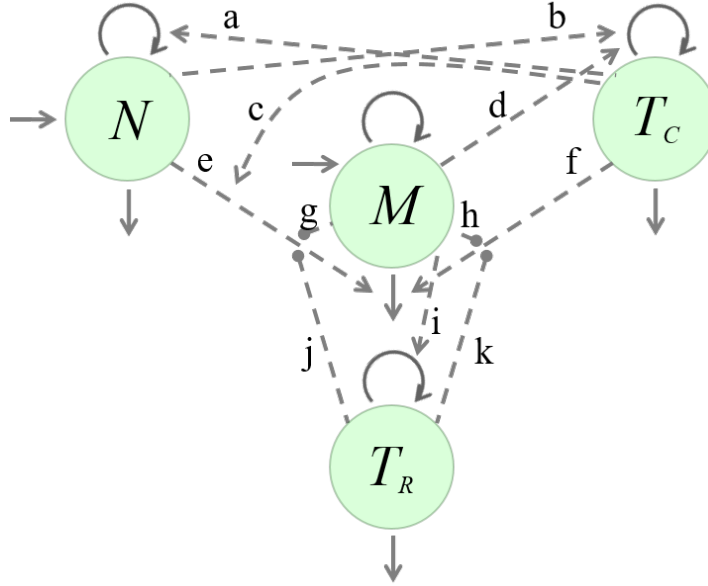


Figure 1 Diagram of population interactions. M represents M protein produced by MM cells, T_C represents CTLs, N represents NK cells, and T_R represents Tregs. The solid curves represent an increase (arrows pointing in) or decrease (arrows only pointing out) in population sizes. The dashed curves represent interactions that either boost (arrows) or inhibit (solid circles) population sizes or rates of change. These interaction pathways (labeled **a – k**) are described in Table 1 and in Section 2.1.

The basic structure of each rate of change equation in our model consists of a constant source rate term s , a logistic growth term with growth rate constant r and carrying capacity K , and a loss term with rate constant δ . We choose logistic growth because of its simplicity among smooth functions that tend toward finite population sizes. Letting P stand for any of the populations M , T_C , N , or T_R , the basic form of the rate of change of P with respect to time t is given by

$$\frac{dP}{dt} = s + rP \left(1 - \frac{P}{K} \right) - \delta P. \tag{1}$$

For the T cell populations, the source term rate constant s , which represents the spontaneous production of T cells that happen to be specific to myeloma, is assumed

Pathway	Description	References
a	T_C crosstalk with N ; boosts N proliferation	[6], [54], [58], [76], [77], [79]
b	N crosstalk with T_C ; boosts T_C proliferation	[6], [65], [76]
c	T_C increases activation/efficacy of N	[54], [58], [77]
d	Antigens shed from M stimulate T_C proliferation	[1], [21], [25], [39], [70], [95]
e	N cells kill myeloma cells and decrease M	[9], [10], [22], [32], [42], [69]
f	T_C cells kill myeloma cells and decrease M	[22], [42], [95]
g	Myeloma cells decrease efficacy of N	[34]
h	Myeloma cells decrease efficacy of T_C	[8], [14], [29], [71], [85]
i	Myeloma cells boost T_R proliferation	[14], [28], [30], [29]
j	T_R decreases efficacy of N	[35], [36], [44], [81], [87], [90]
k	T_R decreases efficacy of T_C	[11], [23], [44], [57], [78], [90]

Table 1 Description of interaction pathways in the model (the dashed curves shown in Fig. 1).

to be insignificant compared to the proliferation rate, and is set to zero. We model feedback between the different populations by modifying the growth rate constant r or the death rate constant δ so that the effective rates increase or decrease in the presence of certain other cell types.

The dynamics of the myeloma cell population, represented by the concentration of M protein in the peripheral blood, M (with units of g/dL), are given by

$$\begin{aligned} \frac{dM}{dt} = & s_M + r_M \left(1 - \frac{M}{K_M}\right) M \\ & - \delta_M \left[1 + \left(\overbrace{\frac{a_{NM}N}{b_{NM} + N}}^e + \overbrace{\frac{a_{CM}T_C}{b_{CM} + T_C}}^f + \overbrace{a_{CNM} \frac{N}{b_{NM} + N} \cdot \frac{T_C}{b_{CM} + T_C}}^c \right) \right. \\ & \left. \left(1 - \overbrace{\frac{a_{MM}M}{b_{MM} + M}}^{g,h} - \overbrace{\frac{a_{RM}T_R}{b_{RM} + T_R}}^{j,k} \right) \right] \cdot M \end{aligned} \quad (2)$$

Significant levels of M protein (up to 1.5 g/dL [63]) can be present in the absence of a MM diagnosis, whereas a Durie-Salmon Stage III diagnosis of MM only requires levels to be greater than 5-7 g/dL [26]. Thus we include a constant source rate for s_M in our model to account for production by normal plasma cells. The terms labeled e and f account for NK cell (N) and CTL (T_C) killing of myeloma cells, respectively. The crosstalk between NK and CTL (pathway c) further increases the efficacy of NK killing of myeloma cells. However, MM (M) and Tregs (T_R) decrease the efficacy of NK and CTL killing of myeloma cells (pathways g , h , j , and k). In the absence of evidence to the contrary, we assume the effect size of pathways g and h are the same. Similarly, we assume the effect size of pathways j and k are the same. We choose saturating functional forms for these interactions (rather than mass action) so that there is a limit to the size of each possible effect.

The rate of change of $T_C(t)$ (measured in units of cells/ μ L) is given by

$$\frac{dT_C}{dt} = r_C \left(1 - \frac{T_C}{K_C}\right) \left(1 + \overbrace{\frac{a_{MC}M}{b_{MC} + M}}^d + \overbrace{\frac{a_{NC}N}{b_{NC} + N}}^b\right) T_C - \delta_C T_C. \quad (3)$$

We assume that antigen shed from myeloma cells is presented to T_C and boosts proliferation (represented by pathway d), and that cytokines secreted by N also lead to increased proliferation of T_C (represented by pathway b). Finally, the rates of change of the populations of NK, $N(t)$, and Tregs, $T_R(t)$, (both measured in units of cells/ μ L) are modeled by

$$\frac{dN}{dt} = s_N + r_N \left(1 - \frac{N}{K_N}\right) \overbrace{\left(1 + \frac{a_{CN}T_C}{b_{CN} + T_C}\right)}^a N - \delta_N N \quad (4)$$

$$\frac{dT_R}{dt} = r_R \left(1 - \frac{T_R}{K_R}\right) \overbrace{\left(1 + \frac{a_{MR}M}{b_{MR} + M}\right)}^i T_R - \delta_R T_R \quad (5)$$

As CTLs and Tregs are part of the adaptive immune response, we assume that their spontaneous production specific to myeloma cells (on the order of 1 out of 10^7 T cells) is negligible in comparison to their proliferation once they initially recognize the myeloma [1]. Thus, we include proliferation terms but not separate source terms for the increase of the CTL and Treg populations. Since the NK cells are part of the innate immune response and do not require specificity to tumor antigens [1], we assume the general production of additional NK cells could contribute significantly to the response of NK cells to myeloma, and include a source term for their increase. Our model also assumes that proliferation of N is increased by crosstalk with T_C (pathway a), and that M increases activation/proliferation of T_R (pathway i). As mentioned above, many of the interactions represented in these equations occur in locations other than the peripheral blood. However, the results of interactions outside the peripheral blood are expected to be reflected in the dynamics of the populations we track within the peripheral blood. The parameters in equations (2) - (5) are described in Table 2.

2.1 Evidence for model pathways

Here, we provide details of all model pathways shown in Fig. 1 and described in Table 1. These pathways represent “net” effects in the system, which may be due to elements not explicitly included in the model. These elements may include cellular components such as T helper, B, and antigen-presenting cells (e.g., dendritic cells), and soluble factors such as cytokines and chemokines that may originate from the immune system, non-immune normal tissue, or tumor. Thus parameters in the system need to be interpreted as “net” effect parameters, which incorporate combined contributions of interactions and elements that are not measured separately.

Also, since we assume levels of and changes to MM cells are reflected in levels of M protein M , effects on or by MM cells are represented by M . Parameters for M may include proportionality constants that relate MM cell levels with M levels.

Pathway a: CTLs boost NK proliferation. Assistance from activated CD8+ T cells in stimulating the proliferation of NK cells has been demonstrated *in vivo* [93].

Pathway b: NK cells boost CTL proliferation. The NK pool boosts effector T cell proliferation through IFN γ secretion from the NK cells, which stimulates dendritic cell (DC) maturation and leads to Th1 polarization of naive T cells, further promoting NK and CTL activation and IFN γ production by direct contact. Additionally, NK killing of target cells boosts DC antigen uptake, antigen presentation by DCs, and subsequent effector T cell proliferation [65].

Pathway c: CTL and NK crosstalk leads to increased MM killing. Assistance from tumor-antigen specific CD4+ and CD8+ T cells in activating anti-tumor response from NK cells has been demonstrated *in vivo* [5, 77]. (CD8 is a co-receptor predominantly found on CTLs.) One possible mechanism for this is the large quantity of interleukin-2 (IL-2), produced by activated CD8+ T cells during an immune response [6]. One clinical study of patients with cancer quantified the extent of activation of NK cells when IL-2 was administered [58]. This pathway results in NK cells having a boosted response to MM, driven by CTL levels.

Pathway d: Myeloma cells stimulate CTL proliferation. Antigens shed from MM cells induce differentiation and expansion of effector T cells (CD4+ and CD8+ T cells) through antigen presentation by DCs [1, 21, 95].

Pathway e: NK cells kill myeloma cells. NK cell killing of myeloma cells has been evidenced *in vitro* and *ex vivo* [9, 32]. This work also attempts to elucidate mechanisms for NK cell recognition of myeloma cells.

Pathway f: CTLs kill myeloma cells. CTL killing of myeloma cells is mediated by perforin secretion, which is responsible for pore formation in cell membranes of target cells [94, 95].

Pathway g: Myeloma cells decrease NK cell efficacy. Human leukocyte antigen-1 (HLA-1, also known as major histocompatibility complex I, or MHC I) expression on myeloma cells confers resistance to lysis by NK cells [34]. PD-1 ligand (PD-L1) on the surface of myeloma cells can down-regulate NK cells through interactions with PD-1 [4]. Also, several additional mechanisms involved in the tumor microenvironment, such as tumor cell-derived factors and tumor-derived exosomes, are immunosuppressive of NK cells [3].

Pathway h: Myeloma cells decrease CTL efficacy. Myeloma cells have been found to express PD-L1, suggesting the PD-L1 binding to PD-1 on CTLs may decrease their cytotoxicity. Anti-PD-1 blocking antibody has been shown to increase CD8+ T cell killing of myeloma cells [37]. Myeloma cells also secrete IL-6 and promote paracrine production of vascular endothelial growth factor (VEGF) by stromal cells [13], which inhibit the differentiation and maturation of DCs and the subsequent priming of T cell activity [33, 59, 72].

Pathway i: Myeloma cells boost Treg proliferation. Myeloma cells can generate inducible Tregs *in vitro* [29], and Treg levels may be higher as a percentage of the CD4+ cells in patients with MM than in healthy adults [28, 30]. Our model

structure causes the Treg levels to increase, but in a bounded manner, as M increases. With respect to *in vivo* data, we point out that in one reference, mean Treg levels are higher in symptomatic MM patients than in the healthy controls [28], while in another reference, mean Treg levels are lower in MM patients than in healthy controls [68]. In both cases, these are mean values, and the variances are high. Given the discrepancies between clinical study data, we reduce the model by assuming that the number of Tregs is constant, as described next in Section 2.2.

Pathway j: Tregs decrease NK efficacy. Tregs can decrease the efficacy of NK cells via transforming growth factor β (TGF- β) in a cell-contact dependent manner [36, 81, 87, 90].

Pathway k: Tregs decrease CTL efficacy. Tregs can decrease the efficacy of CTLs through TGF- β signaling [11, 57]. There is some debate as to whether regulatory T cells also slow the proliferation of cytotoxic T cells in patients with MM [7, 69]. However, Sojka et al. [82] note that the context determines how the regulatory T cells affect their target. In our model, the context is the tumor site. At the tumor site, the primary mechanism of the regulatory T cells is to inhibit CTL efficacy there [11, 57, 90]. Over time, this results in decreased numbers. Therefore, we do not include a specific pathway for decreased CTL proliferation due to regulatory T cells in our model, and focus instead on the primary mechanism of decreased CTL efficacy against the myeloma cells.

2.2 A reduced model for the diseased state

While the full model is comprehensive, it is challenging to analyze mathematically. To gain insight into crucial model components, we focus on the dynamics of two key variables, namely M -protein and CTL levels. Our model reduction is informed by data on the immune cell levels of multiple myeloma patients. Pessoa de Magalhães et al. [68] reported that NK cell levels in the peripheral blood do not vary significantly between patients with various stages of MM, including LTDC and precursor states such as monoclonal gammopathy of unspecified significance (MGUS). Thus, if we focus our attention on individuals already in a diseased state, we can assume that NK levels are approximately constant. In addition, data in Pessoa de Magalhães et al. [68] and Favaloro et al. [28] indicate that the number of Tregs is relatively constant across disease states. To simplify our analysis, we initially restrict our focus to patients with the disease, and assume that NK and Treg levels are fixed at constant steady-state levels.

The reduced model in a diseased state is given by two equations, for M proteins and T_C cells respectively, where \bar{N} and \bar{T}_R are introduced as fixed model parameters. The equations are

$$\begin{aligned}
\frac{dM}{dt} &= s_M + r_M \left(1 - \frac{M}{K_M}\right) M \\
&\quad - \delta_M \left[1 + \left(\frac{a_{NM}\bar{N}}{b_{NM} + \bar{N}} + \frac{a_{CM}T_C}{b_{CM} + T_C} + a_{CNM} \frac{\bar{N}}{b_{NM} + \bar{N}} \cdot \frac{T_C}{b_{CM} + T_C} \right) \right. \\
&\quad \left. \left(1 - \frac{a_{MM}M}{b_{MM} + M} - \frac{a_{RM}\bar{T}_R}{b_{RM} + \bar{T}_R} \right) \right] \cdot M, \\
\frac{dT_C}{dt} &= r_C \left(1 - \frac{T_C}{K_C}\right) \left(1 + \frac{a_{MC}M}{b_{MC} + M} + \frac{a_{NC}\bar{N}}{b_{NC} + \bar{N}} \right) T_C - \delta_C T_C.
\end{aligned} \tag{6}$$

Proofs for existence and uniqueness of solutions for the full and reduced models are given in the Appendix. We list the range of relevant parameter values used in our model in Table 2.

3 Equilibria and Stability

In this section, we show theoretical and numerical analyses for the number of possible equilibrium solutions and their stability properties for the reduced two-dimensional model. From a mathematical perspective, if there exists a unique asymptotically stable positive equilibrium point, then a relevant question will be how it can be moved, through therapy, to reduce the total cancer load. On the other hand, if multiple stable equilibrium points exist (presumably one with a higher cancer load than the others), then the question becomes how one can move the state into the region of attraction of the equilibrium point corresponding to a lower cancer load. For cancer models with tumor-immune system interactions, this is a typical situation (e.g., see [53, 75]). From a practical point of view the results obtained can be interpreted in multiple ways. For example, our results can be used as a diagnostic indicator, helping us to better understand conditions under which patients with MM might enter a state of LTDC or remission.

We recall that, in the reduced model, constant steady-state values \bar{N} for N and \bar{T}_R for T_R are used in the dynamics for M and T_C and we briefly restate the model equations:

$$\begin{aligned}
\frac{dM}{dt} &= s_M + r_M \left(1 - \frac{M}{K_M}\right) M - \delta_M \left[1 + \left(\frac{a_{NM}\bar{N}}{b_{NM} + \bar{N}} + \frac{a_{CM}T_C}{b_{CM} + T_C} \right. \right. \\
&\quad \left. \left. + a_{CNM} \frac{\bar{N}}{b_{NM} + \bar{N}} \cdot \frac{T_C}{b_{CM} + T_C} \right) \left(1 - \frac{a_{MM}M}{b_{MM} + M} - \frac{a_{RM}\bar{T}_R}{b_{RM} + \bar{T}_R} \right) \right] M \\
\frac{dT_C}{dt} &= r_C \left(1 - \frac{T_C}{K_C}\right) \left(1 + \frac{a_{MC}M}{b_{MC} + M} + \frac{a_{NC}\bar{N}}{b_{NC} + \bar{N}} \right) T_C - \delta_C T_C.
\end{aligned}$$

The coefficient a_{CNM} represents the net activation of N that depends on the presence of T_C . Setting

Parameter	Description	Range of Values	References
s_M	Constant source for M	0.005-0.5 g/(dL·day)	Estimated
r_M	Proliferation rate constant for M	0.002-0.05 /day	[2, 18, 40, 64]
K_M	Carrying capacity for M	7-15 g/dL	[68]
δ_M	Basal death/decay rate constant for M	0.006-0.06/day	[38, 60]
a_{NM}	Maximum fold-increase in death rate of M by N	0-10	Estimated
b_{NM}	Threshold for increase in death rate of M by N	$(0-2) \times K_N$	Estimated
a_{CM}	Maximum fold-increase in death rate of M by T_C	0-10	Estimated
b_{CM}	Threshold for increase in death rate of M by T_C	$(0-2) \times K_C$	Estimated
a_{CNM}	Maximum fold-increase in N efficacy by T_C	0-10	Estimated
a_{MM}	Maximum extent M decreases T_C and N efficacy	$a_{MM} + a_{RM} \leq 1$	Estimated
b_{MM}	Threshold for M decreasing T_C and N efficacy	$(0-2) \times K_M$	Estimated
a_{RM}	Maximum extent T_R decreases T_C and N efficacy	$a_{MM} + a_{RM} \leq 1$	Estimated
b_{RM}	Threshold for T_R decreasing T_C and N efficacy	$(0-2) \times K_R$	Estimated
r_C	Proliferation/activation rate constant for T_C	0.01-1/day	[2, 15, 16, 73]
K_C	Carrying capacity for T_C	600-1500 cells/ μ L	[68]
δ_C	Death/inactivation rate constant for T_C	0.5-5/day	[15, 17, 31, 73, 83]
a_{MC}	Maximum fold-increase in activation rate of T_C by M	0-10	Estimated
b_{MC}	Threshold for increase in activation rate of T_C by M	$(0-2) \times K_M$	Estimated
a_{NC}	Maximum fold-increase in activation rate of T_C by N	0-10	Estimated
b_{NC}	Threshold for increase in activation rate of T_C by N	$(0-2) \times K_N$	Estimated
s_N	Constant source rate for N	0.001-5 cells/(μ L·day)	[18, 96]
r_N	Proliferation rate constant for N	0.025-0.2/day	[96]
K_N	Carrying capacity for N	300-650 cells/ μ L	[68]
δ_N	Basal death/inactivation rate constant for N	0.02-0.07/day	[96]
a_{CN}	Maximum fold-increase in activation rate of N by T_C	0-10	Estimated
b_{CN}	Threshold for increase in activation rate of N by T_C	0-1500	Estimated
r_R	Proliferation/activation rate constant for T_R	0.01-0.5/day	[92]
K_R	Carrying capacity for T_R	60-120 cells/ μ L	[68]
δ_R	Basal death/inactivation rate constant for T_R	0.01-0.5/day	[73, 92]
a_{MR}	Maximum fold-increase in activation rate of T_R by M	0-10	Estimated
b_{MR}	Threshold for increase in activation rate of T_R by M	0-15	Estimated
M^0	Observed values of M protein in diseased state	3-10 g/dL	[26]
T_C^0	Observed values of CTLs in diseased state	464 ± 416 cells/ μ L	[68]
N^0	Observed values of NK cells in diseased state	227 ± 141 cells/ μ L	[68]
T_R^0	Observed values of Tregs in diseased state	42 ± 26 cells/ μ L	[68]

Table 2 Table of parameter descriptions and ranges of values used in the model. All parameters are assumed non-negative. M^0, T_C^0, N^0, T_R^0 are used as initial values/conditions.

$$\xi = 1 - \frac{a_{RM}\bar{T}_R}{b_{RM} + \bar{T}_R}, \quad \rho = \frac{\bar{N}}{b_{NM} + \bar{N}} \quad \text{and} \quad \eta = 1 + \frac{a_{NC}\bar{N}}{b_{NC} + \bar{N}},$$

we obtain the following equilibrium equations:

$$0 = s_M + r_M \left(1 - \frac{M}{K_M}\right) M - \delta_M \left[1 + \left(a_{NM}\rho + \frac{(a_{CNM}\rho + a_{CM})T_C}{b_{CM} + T_C}\right) \cdot \left(\xi - \frac{a_{MM}M}{b_{MM} + M}\right)\right] M, \quad (7)$$

$$0 = \left[r_C \left(1 - \frac{T_C}{K_C}\right) \left(\eta + \frac{a_{MC}M}{b_{MC} + M}\right) - \delta_C\right] T_C. \quad (8)$$

We call equilibrium points with $T_C^* = 0$ *trivial* and those with $T_C^* > 0$ *positive*.

3.1 Analysis of trivial equilibrium points: $T_C^* = 0$

In this case, after multiplying equation (7) with $b_{MM} + M$ we obtain that

$$0 = \left(s_M - \delta_M M + r_M \left(1 - \frac{M}{K_M}\right) M\right) (b_{MM} + M) - \delta_M a_{NM}\rho (\xi b_{MM} + (\xi - a_{MM})M) M.$$

This is a cubic polynomial of the form

$$P(M) = -\frac{r_M}{K_M} M^3 + \gamma_2 M^2 + \gamma_1 M + s_M b_{MM}$$

with coefficients

$$\gamma_2 = r_M - \delta_M - b_{MM} \frac{r_M}{K_M} - \delta_M a_{NM}\rho (\xi - a_{MM})$$

and

$$\gamma_1 = s_M + b_{MM} (r_M - \delta_M) - \delta_M a_{NM} b_{MM} \xi \rho.$$

Thus there exists at least one and no more than three positive roots $0 < M_1^* \leq M_2^* \leq M_3^*$. It follows from Descartes' sign rule that there is a unique positive root if either $\gamma_2 < 0$ or $\gamma_1 > 0$. Note that for the dynamics to be meaningful we must have $\xi > a_{MM}$ and thus r_M is the only positive coefficient in γ_2 . However, if $\gamma_2 > 0$ and $\gamma_1 < 0$, then three positive roots are possible. Fig. 2 below, which illustrates the possible scenarios, shows that this is viable.

The stability of trivial equilibrium points is easily established. If we write the dynamics as

$$\frac{dM}{dt} = f_1(M, T_C) \quad \text{and} \quad \frac{dT_C}{dt} = f_2(M, T_C),$$

then for a trivial equilibrium point we have that

$$\frac{\partial f_2}{\partial M}(M^*, 0) = 0$$

and thus the eigenvalues of the Jacobian matrix at $(M^*, 0)$ are given by

$$\frac{\partial f_1}{\partial M}(M^*, 0) \quad \text{and} \quad \frac{\partial f_2}{\partial T_C}(M^*, 0).$$

We have that

$$\frac{\partial f_2}{\partial T_C}(M^*, 0) = r_C \left(\eta + \frac{a_{MC}M^*}{b_{MC} + M^*} \right) - \delta_C \quad (9)$$

and thus $(M^*, 0)$ is unstable if

$$\frac{r_C}{\delta_C} \left(\eta + \frac{a_{MC}M^*}{b_{MC} + M^*} \right) > 1. \quad (10)$$

As the function $M \mapsto \frac{M}{b+M}$ is strictly increasing, there exists a unique *critical value* M_c defined as the solution to the equation

$$\frac{r_C}{\delta_C} \left(\eta + \frac{a_{MC}M}{b_{MC} + M} \right) = 1$$

and given by

$$M_c = \frac{b_{MC} \left(\frac{\delta_C}{r_C} - \eta \right)}{a_{MC} - \left(\frac{\delta_C}{r_C} - \eta \right)}. \quad (11)$$

Trivial equilibrium points $(M^*, 0)$ with $M > M_c$ are unstable. If $M < M_c$, then $\frac{\partial f_1}{\partial M}(M^*, 0)$ determines the overall stability. It follows from $P(M) = (b_{MM} + M)f_1(M, 0)$ that such an equilibrium point is locally asymptotically stable if there is only one positive real root and, if there are three distinct real roots, then the low and high equilibrium points are locally asymptotically stable and the intermediate one is unstable (see Appendix). In particular, the trivial equilibrium closest to the critical value M_c from below is always locally asymptotically stable unless there exists a double root M^* . Then the corresponding eigenvalue is 0 and this equilibrium point is a saddle node while the other equilibrium point is locally asymptotically stable. This fully describes the local stability properties of trivial equilibrium points.

3.2 Number of positive equilibrium points: $T_C^* > 0$

While the trivial equilibrium points are relevant for the overall behavior of the dynamical system, more important are the positive equilibrium points. In this case we have

$$T_C^* = K_C \left(1 - \frac{1}{\frac{r_C}{\delta_C} \left(\eta + \frac{a_{MC}M^*}{b_{MC} + M^*} \right)} \right) \quad (12)$$

and this quantity is positive if and only if $M^* > M_c$. In particular, for the critical value M_c we have that $T_C^* = 0$ and, if the trivial equilibrium point is asymptotically stable for $M < M_c$ near M_c , then this point corresponds to a transcritical or exchange of stability bifurcation between a trivial and a positive equilibrium point. We record the following statement:

Proposition 1. *Positive equilibrium points (M^*, T_C^*) are the equilibrium solutions that lie in the region $\{M > M_c\}$. In this region all trivial equilibrium points are unstable.*

Substituting the formula for T_C^* into equation (7) gives

$$0 = s_M - \delta_M M + r_M \left(1 - \frac{M}{K_M}\right) M \quad (13)$$

$$- \delta_M \left(a_{NM} \rho + \frac{(a_{CM} + a_{CNM} \rho) K_C \left(1 - \frac{1}{\frac{r_C}{\delta_C} \left(\eta + \frac{a_{MC} M}{b_{MC} + M}\right)}\right)}{b_{CM} + K_C \left(1 - \frac{1}{\frac{r_C}{\delta_C} \left(\eta + \frac{a_{MC} M}{b_{MC} + M}\right)}\right)} \right) \left(\xi - \frac{a_{MM} M}{b_{MM} + M} \right) M.$$

Fractional linear transformations form a group under composition and thus this last term is still a fractional linear transformation. Algebraic manipulations (which are included in the Appendix) lead to the following expression:

$$a_{NM} \rho + \frac{(a_{CNM} \rho + a_{CM}) K_C \left(1 - \frac{1}{\frac{r_C}{\delta_C} \left(\eta + \frac{a_{MC} M}{b_{MC} + M}\right)}\right)}{b_{CM} + K_C \left(1 - \frac{1}{\frac{r_C}{\delta_C} \left(\eta + \frac{a_{MC} M}{b_{MC} + M}\right)}\right)} = \frac{\beta_0 + \beta_1 M}{\alpha_0 + \alpha_1 M} \quad (14)$$

where

$$\alpha_0 = b_{MC} \left[(b_{CM} + K_C) \frac{r_C}{\delta_C} \eta - K_C \right],$$

$$\alpha_1 = (b_{CM} + K_C) \frac{r_C}{\delta_C} (\eta + a_{MC}) - K_C,$$

$$\beta_0 = b_{MC} \left\{ a_{NM} \rho b_{CM} \frac{r_C}{\delta_C} \eta + ((a_{CNM} + a_{NM}) \rho + a_{CM}) K_C \left(\frac{r_C}{\delta_C} \eta - 1 \right) \right\},$$

$$\beta_1 = a_{NM} b_{CM} \rho \frac{r_C}{\delta_C} (\eta + a_{MC}) + ((a_{CNM} + a_{NM}) \rho + a_{CM}) K_C \left[\frac{r_C}{\delta_C} (\eta + a_{MC}) - 1 \right].$$

Note that

$$\alpha_0 > 0 \Leftrightarrow \frac{r_C}{\delta_C} \eta > \frac{K_C}{b_{CM} + K_C}, \quad \text{and} \quad \alpha_1 > 0 \Leftrightarrow \frac{r_C}{\delta_C} (\eta + a_{MC}) > \frac{K_C}{b_{CM} + K_C}.$$

In particular, if α_0 is positive, then so is α_1 . Furthermore, if $\frac{r_C}{\delta_C}\eta > 1$, then actually all these coefficients (including β_0 and β_1) are positive. If T_C is small, then $\frac{r_C}{\delta_C}\eta > 1$ simply means that the CTLs do not die out which would seem to be a biologically reasonable assumption. In any case, we always have the following result:

Lemma 1. *For $M \geq M_c$ we always have that $\alpha_0 + \alpha_1 M > 0$.*

Proof. If $M > M_c$ then the following holds

$$b_{MC} \left(\frac{r_C}{\delta_C} \eta - 1 \right) + \left[\frac{r_C}{\delta_C} (\eta + a_{MC}) - 1 \right] M > 0. \quad (15)$$

Hence

$$\begin{aligned} \alpha_0 + \alpha_1 M &= b_{MC} \left[(b_{CM} + K_C) \frac{r_C}{\delta_C} \eta - K_C \right] + \left[(b_{CM} + K_C) \frac{r_C}{\delta_C} (\eta + a_{MC}) - K_C \right] M \\ &= b_{CM} \frac{r_C}{\delta_C} [\eta(b_{MC} + M) + a_{MC}M] + K_C \left\{ b_{MC} \left(\frac{r_C}{\delta_C} \eta - 1 \right) \right. \\ &\quad \left. + \left[\frac{r_C}{\delta_C} (\eta + a_{MC}) - 1 \right] M \right\} \\ &> 0. \end{aligned}$$

The first term is always positive and thus this also holds in a neighborhood of $M = M_c$. \square

Overall, equation (13) is therefore equivalent to

$$0 = s_M - \delta_M M + r_M \left(1 - \frac{M}{K_M} \right) M - \delta_M \left(\frac{\beta_0 + \beta_1 M}{\alpha_0 + \alpha_1 M} \right) \left(\frac{\xi b_{MM} + (\xi - a_{MM})M}{b_{MM} + M} \right) M.$$

Multiplying this equation by $(\alpha_0 + \alpha_1 M)(b_{MM} + M) > 0$ gives

$$\begin{aligned} 0 &= \left(s_M - \delta_M M + r_M \left(1 - \frac{M}{K_M} \right) M \right) (\alpha_0 + \alpha_1 M)(b_{MM} + M) \\ &\quad - \delta_M (\beta_0 + \beta_1 M) (\xi b_{MM} + (\xi - a_{MM})M) M. \end{aligned} \quad (16)$$

This relation defines a fourth-order polynomial Q of the form

$$Q(M) = \omega_4 M^4 + \omega_3 M^3 + \omega_2 M^2 + \omega_1 M + \omega_0$$

with coefficients

$$\begin{aligned}
\omega_4 &= -\alpha_1 \frac{r_M}{K_M}, \\
\omega_3 &= (r_M - \delta_M)\alpha_1 - \frac{r_M}{K_M}(\alpha_0 + \alpha_1 b_{MM}) - \delta_M \beta_1 (\xi - a_{MM}), \\
\omega_2 &= s_M \alpha_1 + (r_M - \delta_M)(\alpha_0 + \alpha_1 b_{MM}) - \frac{r_M}{K_M} \alpha_0 b_{MM} - \delta_M \beta_1 \xi b_{MM} - \delta_M \beta_0 (\xi - a_{MM}), \\
\omega_1 &= s_M(\alpha_0 + \alpha_1 b_{MM}) + (r_M - \delta_M)\alpha_0 b_{MM} - \delta_M \beta_0 \xi b_{MM}, \\
\omega_0 &= \alpha_0 b_{MM} s_M.
\end{aligned}$$

If α_0 is positive, then there exist at least one positive and one negative real root for Q . Hence in this case there are at most three positive real roots for M . In principle, if α_0 is negative and α_1 is positive, then there could exist four real roots. However, we are only interested in solutions $M > M_c$ and there is no a priori guarantee that such solutions exist. We summarize these observations in the following proposition.

Proposition 2. *Each root $M^* > M_c$ of $Q(M) = 0$ defines a positive equilibrium point. In general, there are at most four positive roots of Q while there exist at most three positive solutions if α_0 is positive. In this case there exists at least one positive equilibrium solution (M^*, T_C^*) if $Q(M_c) > 0$, and the latter holds if and only if $f_1(M_c, 0) > 0$.*

Proof. The statements about the number of positive solutions have already been verified and, if $\alpha_0 > 0$, it is clear from the mean value theorem that a solution $M > M_c$ exists if $Q(M_c) > 0$. As the value M_c corresponds to the bifurcation point when the positive equilibrium point T_C^* becomes zero, it follows from equation (14) that $a_{NM}\rho = \frac{\beta_0 + \beta_1 M_c}{\alpha_0 + \alpha_1 M_c}$ and thus $Q(M_c)$ is positive if and only if the dynamics for M at the point $(M, T_C) = (M_c, 0)$ are positive, i.e.,

$$\left. \frac{dM}{dt} \right|_{M=M_c, T_C=0} = f_1(M_c, 0) > 0.$$

This proves the result. \square

3.3 Stability of positive equilibrium points: $T_C^* > 0$

Recall that

$$\begin{aligned}
f_1(M, T_C) &= s_M - \delta_M M + r_M \left(1 - \frac{M}{K_M}\right) M \\
&\quad - \delta_M \left(a_{NM}\rho + (a_{CNM}\rho + a_{CM}) \frac{T_C}{b_{CM} + T_C} \right) \left(\xi - \frac{a_{MM}M}{b_{MM} + M} \right) M, \\
f_2(M, T_C) &= r_C \left(1 - \frac{T_C}{K_C}\right) \left(\eta + \frac{a_{MC}M}{b_{MC} + M} \right) T_C - \delta_C T_C.
\end{aligned}$$

The Jacobian matrix at an equilibrium point (M^*, T_C^*) is given by

$$A = \begin{pmatrix} \frac{\partial f_1}{\partial M}(M^*, T_C^*) & \frac{\partial f_1}{\partial T_C}(M^*, T_C^*) \\ \frac{\partial f_2}{\partial M}(M^*, T_C^*) & \frac{\partial f_2}{\partial T_C}(M^*, T_C^*) \end{pmatrix} \quad (17)$$

and the equilibrium point is locally asymptotically stable if and only if the trace of the Jacobian is negative and the determinant is positive. This is elementary and also follows from the Routh-Hurwitz criterion.

Except for the $(1, 1)$ -term in A , all other terms have constant signs (regardless of the parameter values). We have that

$$\begin{aligned} \frac{\partial f_2}{\partial M}(M^*, T_C^*) &= r_C \left(1 - \frac{T_C^*}{K_C}\right) \frac{a_{MC} b_{MC}}{(b_{MC} + M^*)^2} T_C^* \\ &= \frac{\delta_C a_{MC} b_{MC} T_C^*}{(\eta(b_{MC} + M^*) + a_{MC} M^*)(b_{MC} + M^*)} > 0, \end{aligned} \quad (18)$$

$$\begin{aligned} \frac{\partial f_2}{\partial T_C}(M^*, T_C^*) &= -\frac{r_C}{K_C} \left(\eta + \frac{a_{MC} M^*}{b_{MC} + M^*}\right) T_C^* \\ &= \delta_C - r_C \left(\eta + \frac{a_{MC} M^*}{b_{MC} + M^*}\right) < 0, \end{aligned} \quad (19)$$

and

$$\frac{\partial f_1}{\partial T_C}(M^*, T_C^*) = -\delta_M (a_{CNM}\rho + a_{CM}) \frac{b_{CM}}{(b_{CM} + T_C^*)^2} \left(\xi - \frac{a_{MM} M^*}{b_{MM} + M^*}\right) M^* < 0 \quad (20)$$

where the last inequality is an immediate consequence of the meaning of the dynamics. Also note that the gradient of f_2 vanishes at the critical point $(M^*, T_C^*) = (M_C, 0)$ in agreement with the character of this point as a bifurcation point. For positive equilibria, the signs above imply the following statement:

Proposition 3. *A positive equilibrium point (M^*, T_C^*) for which $\frac{\partial f_1}{\partial M}(M^*, T_C^*)$ is negative is locally asymptotically stable.*

While this is only a sufficient condition, it is quite useful for this model. Numerically it is easy to compute the trace and determinant and thus check any particular point. The $(1, 1)$ -term in A is given by

$$\begin{aligned} \frac{\partial f_1}{\partial M}(M^*, T_C^*) &= r_M - \delta_M - 2\frac{r_M}{K_M} M^* - \delta_M \left(a_{NM}\rho + (a_{CNM}\rho + a_{CM}) \frac{T_C^*}{b_{CM} + T_C^*} \right) \\ &\quad \cdot \left(\xi - \frac{a_{MM} M^*}{b_{MM} + M^*} - \frac{a_{MM} b_{MM} M^*}{(b_{MM} + M^*)^2} \right). \end{aligned}$$

Using the equilibrium condition

$$\delta_M \left(a_{NM}\rho + (a_{CNM}\rho + a_{CM}) \frac{T_C^*}{b_{CM} + T_C^*} \right) \left(\xi - \frac{a_{MM}M^*}{b_{MM} + M^*} \right) = \frac{s_M}{M^*} - \delta_M + r_M \left(1 - \frac{M^*}{K_M} \right),$$

this simplifies to

$$\frac{\partial f_1}{\partial M}(M^*, T_C^*) = -\frac{s_M}{M^*} - \frac{r_M}{K_M} M^* + \delta_M \left(a_{NM}\rho + (a_{CNM}\rho + a_{CM}) \frac{T_C^*}{b_{CM} + T_C^*} \right) \frac{a_{MM}b_{MM}M^*}{(b_{MM} + M^*)^2}$$

with the first two terms negative and the last term positive. As $M^* \rightarrow \infty$, the equilibrium solution $T_C^* = T_C^*(M^*)$ approaches its steady-state value

$$K_C \left(1 - \frac{1}{\frac{r_C}{\delta_C} (\eta + a_{MC})} \right)$$

and thus the linear term dominates. Hence, if M^* is large enough, this partial derivative is negative and a positive equilibrium point will always be locally asymptotically stable.

3.4 Numerical illustration and interpretation of the results

We illustrate the model results with phase portraits shown in Fig. 2. The number of equilibrium points, as well as their stability, are consistent with what has been described in the theoretical analysis above. The parameters that were kept constant in all of these simulations are summarized in the caption of Fig. 2. The only parameter that is varied is a_{CNM} and its value is also given in the caption. We chose to increase the parameter a_{CNM} as a proof of concept to illustrate the bistable behavior of our model (a feature also found in other tumor-immune models). Similar to the study of Sontag [83], we highlight how a relatively simple model can recapitulate some of the basic features of interactions between the immune system and myeloma cells.

In Fig. 2, we show that the model exhibits bistability. As stated previously, bistability can be interpreted as a situation in which, depending on the T_C and M levels, we can predict whether an individual is more likely to enter a state of LTDC (represented by a lower stable equilibrium value M), or approach a state of higher tumor burden (a higher stable equilibrium value for M). Starting with a base set of parameters, as shown in Fig. 2(a), high tumor burden is likely, regardless of the initial T_C and M levels. However, as we increase the parameter a_{CNM} (so, as we increase T_C 's activation of N), LTDC becomes possible. In particular, Figs. 2(b) and (c) illustrate a bistable state where, depending on the initial condition (i.e., the T_C and M levels), a state of high tumor burden or LTDC is possible. Lower values of a_{CNM} , as in Fig. 2(b), correspond to a smaller basin of attraction for the lower level stable disease. Higher values of a_{CNM} , as in Fig. 2(c), correspond to a larger ‘‘favorable basin’’.

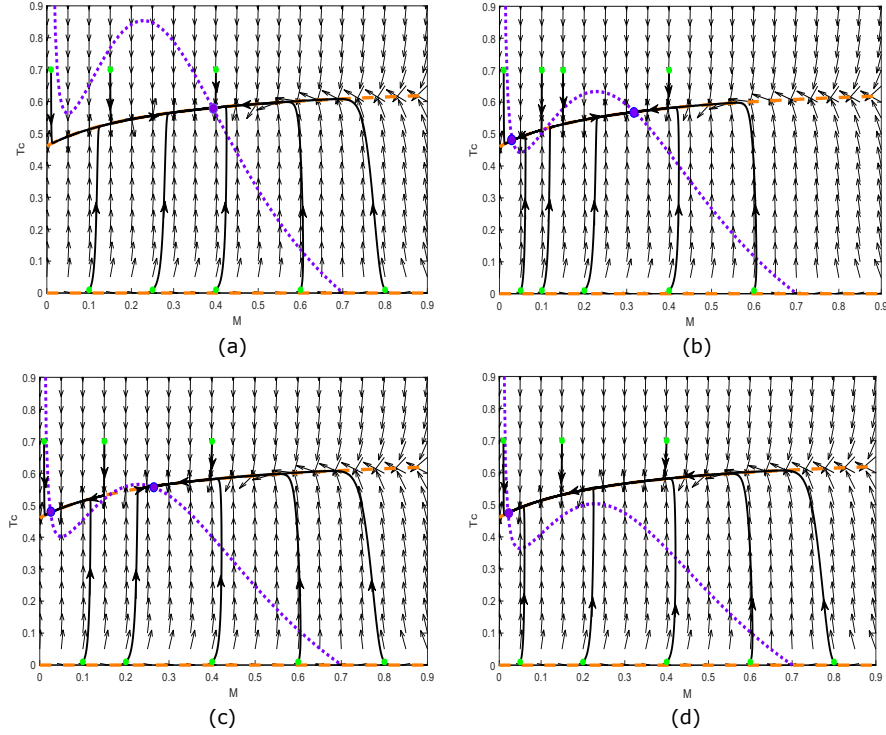


Figure 2 Phase portraits illustrating the bistable behavior of the reduced model (population levels divided by their carrying capacities). In each figure, the green dots correspond to initial conditions, the black lines correspond to trajectories over time, and the purple dots correspond to stable equilibrium points. The orange dashed and purple dotted curves show the T_C - and M -nullclines, respectively, which are defined by the equilibrium equations (7) and (8). (a) $a_{CNM} = 24$: High tumor burden (one stable high MM equilibrium); (b) $a_{CNM} = 28.5$ and (c) $a_{CNM} = 30.6$: Bistability, such that an increase in a_{CNM} results in a larger basin of attraction of the low MM equilibrium (LTDC); (d) $a_{CNM} = 33$: LTDC (one stable low MM equilibrium). Other parameter values are: $r_M = 0.05$, $\delta_M = 0.012$, $s_M = 0.0005$, $r_C = 0.6$, $\delta_C = 0.5$, $\bar{N} = 0.6$, $\bar{T}_R = 1.5$, $a_{NM} = 6$, $b_{NM} = 0.5$, $a_{MM} = 0.35$, $b_{MM} = 0.1$, $a_{RM} = 0.64$, $b_{RM} = 0.1$, $a_{CM} = 6$, $b_{CM} = 0.5$, $a_{MC} = 1$, $b_{MC} = 0.5$, $a_{NC} = 1$, and $b_{NC} = 0.5$.

These results suggest that, as a_{CNM} is increased, the probability of moving to a state of high tumor burden is less likely, but depends on the M and T_C levels. Fig. 2(d) shows the effect of further increasing a_{CNM} . Here, the bistable state is lost, and individuals end up in a state of LTDC, starting from any M and T_C levels. We get the same qualitative results, starting with the parameters used in Fig. 2(a), by either lowering \bar{T}_R or increasing \bar{N} (results not shown). These results are consistent with what we might expect biologically. In particular, if we increase the N cell count sufficiently high (keeping T_R fixed), or if we reduce the T_R cell count (while fixing the N cell count), we see that the high tumor burden state for M becomes smaller

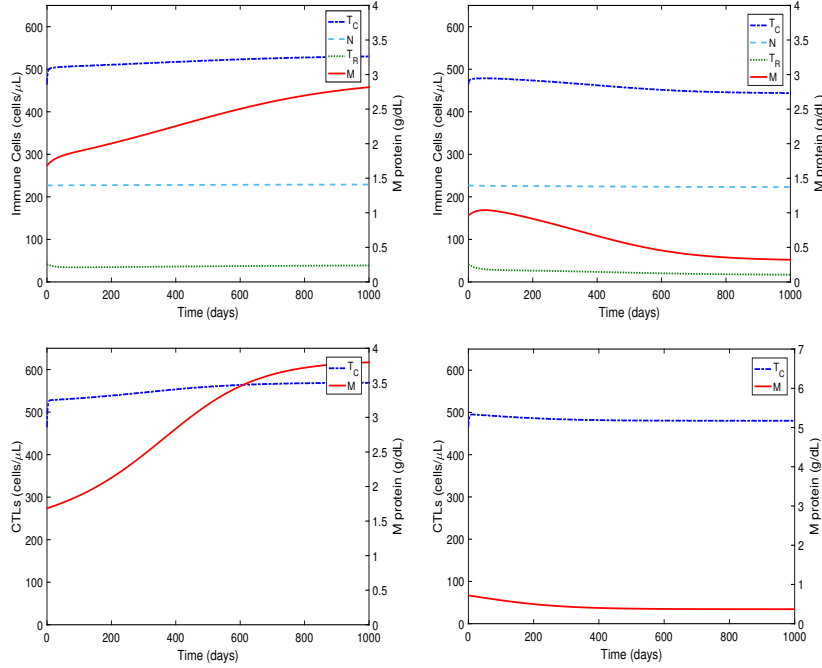


Figure 3 Both the full (top) and reduced (bottom) models show bistability when the initial condition for M protein is varied. Initial conditions for immune cells that correspond to a diseased state [68] are $T_C(0) = 464$, $N(0) = 227$, and $T_R(0) = 42$. Scale on the left of each plot corresponds to immune cells T_C , N , and T_R , and scale on the right of each plot corresponds to M-protein concentration (illustrated by solid red curves). **Top left:** $M(0) = 1.68$ and **Top right:** $M(0) = 0.72$. **Bottom:** Simulation of reduced model. **Bottom left:** $M(0) = 1.62$, $T_C(0) = 252$ and **Bottom right:** $M(0) = 0.72$, $T_C(0) = 252$. All non-scaled parameter values for the **full simulation** are: $r_M = 0.05$, $\delta_M = 0.012$, $s_M = 0.006$, $r_C = 0.6$, $\delta_C = 0.5$, $r_N = 0.02$, $\delta_N = 0.025$, $s_N = 1.49$, $r_R = 0.0831$, $\delta_R = 0.0757$, $b_{NM} = 0.5 * K_N$, $b_{CM} = 0.5 * K_C$, $b_{MM} = 0.1 * K_M$, $b_{RM} = 0.1 * K_R$, $b_{MC} = 0.5 * K_M$, $b_{NC} = 0.5 * K_N$, $b_{CN} = 0.375 * K_C$, $b_{MR} = 0.25 * K_M$, $a_{NM} = 6$, $a_{CM} = 6$, $a_{CNM} = 16$, $a_{MM} = 0.35$, $a_{RM} = 0.64$, $a_{MC} = 1$, $a_{NC} = 1$, $a_{CN} = 1$, $a_{MR} = 1$. The carrying capacities are: $K_M = 12$, $K_C = 1000$, $K_N = 550$, and $K_R = 100$.

(the highest stable equilibrium in Fig. 2(b) is shifted to the left) and the basin of attraction for the LTDC state becomes larger. If we further decrease the T_R level (or increase N) we arrive again at a state of LTDC. We should point out that these are just example parameter sets. To gain more specific insight into the model dynamics, model parameterization and sensitivity analysis should be completed.

In Fig. 3, we compare the full (top) and reduced (bottom) models. When initial M-protein values are varied (keeping all other parameters fixed), we observe a *switch* between high tumor burden and LTDC. This bistability is observed in both the full and reduced models, demonstrating that the underlying dynamics of bistability are well captured by our model reduction, despite Tregs and NK cells being

held constant. This indicates that the model reduction has good predictive power overall, but the full model can display rich dynamics that we will examine further in the future.

In Fig. 3 (top left), we initialize M-protein levels to a value of 1.68 g/dL. In this case, we note that the M protein approaches a diseased steady-state value of 2.95 g/dL (achieved in around 1200 days), with steady-state values for the immune cell populations of 533, 229, and 39 cells/ μ L for CTLs, NK cells, and Tregs, respectively. In Fig. 3 (top right), we initialize the M-protein level at 0.72 g/dL. Note that there is an initial immune response, in which the CTL population increases. Eventually, the M-protein levels decrease to a value of 0.306 g/dL and the immune response is decreased (evidenced by a drop in the CTL population). In this case, steady-state values for the immune cell populations are 443, 223, and 17 cells/ μ L for CTLs, NK cells, and Tregs, respectively. In both cases (diseased and LTDC), NK cells do not change much. This result is consistent with the work of Pessoa de Magalhães et al. [68], in which NK cells are approximately 230 cells/ μ L in both diseased and LTDC states. However, CTLs are higher in the case of LTDC [68]. Similar to our bistable results, these results indicate that a potential mechanism for controlling myeloma level is due to a decrease in the Treg population.

The corresponding reduced two-dimensional model is shown in Fig. 3 (bottom). We note a similar bistable *switch*. In both cases, we start with the same initial conditions used in the full simulation for M protein and CTLs, and note similar trends in the long-term dynamics of both populations. In Fig. 3 (bottom left), we find steady-state values of M protein and CTLs to be 3.82 g/dL and 569 cells/ μ L, respectively (as compared to 2.95 g/dL and 533 cells/ μ L in the full simulation). In Fig. 3 (bottom right) we find steady-state values of M protein and CTLs to be 0.308 g/dL and 480 cells/ μ L, respectively (as compared to 0.306 g/dL and 433 cells/ μ L in the full simulation).

In these numerical examples, steady state is attained in two to three years. In other simulations [not shown], we saw times to steady state that were both higher and lower than these, with more that were lower. The clinical time course for the progression of the disease from asymptomatic with low M-protein levels to a higher M-protein level with symptoms requiring therapy is highly variable. In a review of 1027 newly-diagnosed patients, the median survival duration was less than three years [51]. For comparison, consider monoclonal gammopathy of undetermined significance (MGUS), a state in which M-protein levels are low and patients are asymptomatic. The risk of progression from MGUS to multiple myeloma occurs at a rate of roughly 1% per year [50]. Smoldering multiple myeloma (SMM), another asymptomatic state, has higher M-protein levels (≥ 3 g/dL [50]). SMM patients have a 10% annual risk of progressing to MM for the first five years following diagnosis [49]. At these rates, it would take an average of about 6.5 years for a patient to progress from SMM to MM, and longer to progress from MGUS to MM. The range of time scales observed in our simulations suggests that the parameter sets we used may be more likely to match patients starting with MM or SMM, rather than MGUS.

4 Conclusion and Future Work

In this paper, we formulated a mathematical model for in-host, MM tumor-immune system interactions. The full model includes four populations: M proteins, CTLs, NK cells, and Tregs. The interactions of these four populations represented in the model include key pathways that regulate the crosstalk between MM cells and immune system cells. The model is set in the peripheral blood, which means it can be calibrated to data from peripheral blood samples, although many of the interactions represented in the model reflect actions that occur elsewhere. Based on experimental evidence from the literature, we perform analysis on a reduced system in which NK cell and Treg populations are roughly constant in the disease state. Thus, we can set their rates of change to zero, and N and T_R take on constant values. This simplifies the model to a system of two differential equations: one for M proteins and one for CTLs. The resulting reduced model for M proteins includes the role of CTLs and NK cells in enhancing the removal of M proteins (and also includes CTLs increasing the activation of NK cells). Further, inhibitory effects of M proteins and Tregs on M protein loss are also included. The reduced model for CTLs includes the role of M proteins and NK cells that enhance the growth rate of CTLs.

The theoretical and numerical analysis of the reduced model demonstrates that there are regions of parameter space for which the system allows for the existence of two stable, non-zero equilibrium points. Depending on initial values for M protein and CTLs, the long-term behavior of the model may be LTDC, or may be a state of high disease burden. If the model is validated, then knowing the initial cell counts, we could predict if a patient will likely enter a state of LTDC or high disease burden. Further, once tumor control therapies are added (future work described below), we can address questions such as how to move from an undesired high M-protein state (indicative of high tumor burden) to a more favorable LTDC state.

Our analysis indicates that the system behavior may be sensitive to the value of the parameter that describes CTLs increasing NK cell activation (the parameter a_{CNM}). Specifically, in cases of high a_{CNM} , a stable, low M-protein level equilibrium emerges, with a basin of attraction that increases as CTL activation of NK cells increases. This shows that an immune-controlled state, corresponding to LTDC is possible in our model, but it requires that either CTLs are extremely effective at activating NK cells or that there are a large number of CTLs to achieve a similar effect. Similar bistable results give a state of LTDC if we have a sufficiently high number of NK cells or a sufficiently low number of Treg cells.

Our findings are in qualitative agreement with data. In Pessoa de Magalhães [68], a careful examination of the distribution of various classes of lymphocytes in the peripheral blood of patients with MM who had achieved LTDC revealed differences in the immune cell composition between healthy adults and patients in various stages of progression toward MM. In particular, long-term controlled patients with MM had higher numbers of CD8+ T cells and NK cells. Our analysis results suggesting that CTLs are key components of immune control in patients with MM agree with these clinical observations. Further, our model predicted that a low M-protein level

steady state would be stable if NK cell levels are increased, indicating the importance of the innate immune system in achieving long-term remission.

This work constitutes a first stage in the analysis of the full model. It is a natural question to ask whether the analysis of the equilibria and stability completed for the reduced two-dimensional (2D) model will tell us anything about the dynamical properties of the full four-dimensional (4D) system. This answer is not an easy one, as the full system dynamics are highly nonlinear. Analysis of the reduced model only provides information for a 2D slice of the 4D model, in which two variables, NK cells and Tregs, are taken at their steady-state values. We might expect that, for values close to these steady-state values, the model behavior will remain similar. However, for values far from the steady-state values, the behavior may be quite different. The model reduction used here (fixing NK cells and Tregs at their steady-state values) was motivated by data from the literature. As stated in Section 2.2, multiple sources show that both Treg and NK cell populations do not change much during the progression of MM [68, 28]. Thus, we expect that the analysis performed in this paper will be of use in understanding the long-term behavior of the full system.

In addition to our study lacking the full model dynamics, our current model does not include the effects of therapy. However, there are several types of drugs that are designed to boost immune responses [46] and their role in achieving long-term remission can be explored with this model. Future work will be conducted to clearly define how each of these drugs acts on the model pathways outlined in this paper. The ultimate goal of that work will be to introduce therapy in a full MM tumor–immune model and examine whether optimal dosing strategies can move states with high M-protein levels into a region of attraction of LTDC.

5 Appendix

In this section, we include formal calculations that were omitted in the main text.

Existence and Uniqueness of Solutions

Here, we discuss an existence and uniqueness result for the full model given by equations (2) through (5), and the reduced model given by system (6).

Proposition 4. *Given an initial condition (M^0, T_C^0, N^0, T_R^0) in the closed first quadrant*

$$Q = \{(M, T_C, N, T_R) : M \geq 0, T_C \geq 0, N \geq 0, T_R \geq 0\},$$

the differential equations defined by equations (2) through (5) have a unique solution which exists for all times $t \geq 0$ and lies in Q .

Proof. The right-hand side of this differential equation is continuously differentiable in a neighborhood of Q and thus for initial conditions in Q locally there exists a unique solution. As $T_C \equiv 0$ and $T_R \equiv 0$ are equilibrium solutions and as $\frac{dM}{dt}|_{M=0}$ and $\frac{dN}{dt}|_{N=0}$ have source terms and thus are positive, it follows that Q is positively invariant, i.e., solutions that start in Q will remain in Q throughout their interval of existence. Finally, since all the Michaelis-Menten type expressions of the form $\frac{ax}{b+x}$ with $x \in \{M, T_C, N, T_R\}$ are bounded, it follows that there exist constants $C_1, C_2, C_3,$ and C_4 such that

$$\left| \frac{dM}{dt} \right| \leq s_M + C_1 M, \quad \left| \frac{dT_C}{dt} \right| \leq C_3 T_C,$$

and

$$\left| \frac{dN}{dt} \right| \leq s_N + C_2 N, \quad \left| \frac{dT_R}{dt} \right| \leq C_4 T_R,$$

hold. Hence each of these quantities grow at most exponentially and thus solutions exist for all times. \square

Analogous to the full model, we have the following existence and uniqueness result for the reduced system (6):

Proposition 5. *Given an initial condition (M^0, T_C^0) in the closed first quadrant $Q = \{(M, T_C) : M \geq 0, T_C \geq 0\}$, the differential equations (6) have a unique solution which exists for all times $t \geq 0$ and lies in Q .*

Scaled model

To reduce the number of unknown parameters, we perform the following scaling: $M^* = M/K_M, N^* = N/K_N, T_C^* = T_C/K_C,$ and $T_R^* = T_R/K_R.$

$$\begin{aligned} \frac{dM^*}{dt} &= \frac{s_M}{K_M} + r_M(1 - M^*)M^* - \delta_M \left[1 + \left(\frac{a_{NM}N^*}{b_{NM}/K_N + N^*} + \frac{a_{CM}T_C^*}{b_{CM}/K_C + T_C^*} \right. \right. \\ &\quad \left. \left. + a_{CNM} \frac{N^*}{b_{NM}/K_N + N^*} \cdot \frac{T_C^*}{b_{CM}/K_C + T_C^*} \right) \left(1 - \frac{a_{MM}M^*}{b_{MM}/K_M + M^*} - \frac{a_{RM}T_R^*}{b_{RM}/K_R + T_R^*} \right) \right] M^* \\ \frac{dT_C^*}{dt} &= r_C(1 - T_C^*) \left(1 - \frac{a_{MC}M^*}{b_{MC}/K_M + M^*} + \frac{a_{NC}N^*}{b_{NC}/K_N + N^*} \right) T_C^* - \delta_C T_C^* \\ \frac{dN^*}{dt} &= \frac{s_N}{K_N} + r_N(1 - N^*) \left(1 + \frac{a_{CN}T_C^*}{b_{CN}/K_C + T_C^*} \right) N^* - \delta_N N^* \\ \frac{dT_R^*}{dt} &= r_R(1 - T_R^*) \left(1 + \frac{a_{MR}M^*}{b_{MR}/K_M + M^*} \right) T_R^* - \delta_R T_R^* \end{aligned}$$

Dropping asterisks and introducing the notation $\bar{s}_M = s_M/K_M, \bar{b}_{NM} = b_{NM}/K_N,$ $\bar{b}_{CM} = b_{CM}/K_C,$ etc., we obtain

$$\begin{aligned}
\frac{dM}{dt} &= \bar{s}_M + r_M(1-M)M - \delta_M \left[1 + \left(\frac{a_{NM}N}{\bar{b}_{NM}+N} + \frac{a_{CM}T_C}{\bar{b}_{CM}+T_C} \right. \right. \\
&\quad \left. \left. + a_{CNM} \frac{N}{\bar{b}_{NM}+N} \cdot \frac{T_C}{\bar{b}_{CM}+T_C} \right) \left(1 - \frac{a_{MM}M}{\bar{b}_{MM}+M} - \frac{a_{RM}T_R}{\bar{b}_{RM}+T_R} \right) \right] M \\
\frac{dT_C}{dt} &= r_C(1-T_C) \left(1 - \frac{a_{MC}M}{\bar{b}_{MC}+M} + \frac{a_{NC}N}{\bar{b}_{NC}+N} \right) T_C - \delta_C T_C \\
\frac{dN}{dt} &= \bar{s}_N + r_N(1-N) \left(1 + \frac{a_{CN}T_C}{\bar{b}_{CN}+T_C} \right) N - \delta_N N \\
\frac{dT_R}{dt} &= r_R(1-T_R) \left(1 + \frac{a_{MR}M}{\bar{b}_{MR}+M} \right) T_R - \delta_R T_R
\end{aligned}$$

Based on this scaling, we restrict the values of all scaled threshold parameters \bar{b}_{pq} ($p, q = M, N, C$, or R), to be between 0 and 2 (i.e., much smaller or twice the population carrying capacity).

Stability of trivial equilibria for $M < M_c$

Recall that $P(M) = (b_{MM} + M)f_1(M, 0)$ and thus we have that

$$P'(M^*) = f_1(M^*, 0) + (b_{MM} + M^*) \frac{\partial f_1}{\partial M}(M^*, 0) = (b_{MM} + M^*) \frac{\partial f_1}{\partial M}(M^*, 0).$$

Hence the second eigenvalue has the same sign as $P'(M^*)$.

If there is only one positive real root, then this equilibrium point is locally asymptotically stable: Ignoring the positive factor $\frac{r_M}{K_M}$, if the complex roots are $\alpha \pm i\beta$, then we have that

$$P(M) = -(M - M^*) [(M - \alpha)^2 + \beta^2],$$

and thus

$$P'(M^*) = - [(M^* - \alpha)^2 + \beta^2] < 0.$$

If there are three distinct real roots $0 < M_1^* < M_2^* < M_3^*$,

$$P(M) = -(M - M_1^*)(M - M_2^*)(M - M_3^*),$$

then the low and high equilibrium points are locally asymptotically stable and the intermediate one is unstable. This simply follows from

$$\begin{aligned}
P'(M_1^*) &= -(M_1^* - M_2^*)(M_1^* - M_3^*) < 0, \\
P'(M_2^*) &= -(M_2^* - M_1^*)(M_2^* - M_3^*) > 0, \\
P'(M_3^*) &= -(M_3^* - M_1^*)(M_3^* - M_2^*) < 0.
\end{aligned}$$

In particular, the trivial equilibrium closest to the critical value M_c from below is always locally asymptotically stable except when there exists a double root M^* .

Then the corresponding eigenvalue is 0 and this equilibrium point is a saddle-node while the other equilibrium point is locally asymptotically stable.

Algebraic simplification for positive equilibria

We verify equation (14):

$$\begin{aligned}
& \frac{K_C \left(1 - \frac{1}{\frac{r_C}{\delta_C} \left(\eta + \frac{a_{MC}M}{b_{MC}+M} \right)} \right)}{b_{CM} + K_C \left(1 - \frac{1}{\frac{r_C}{\delta_C} \left(\eta + \frac{a_{MC}M}{b_{MC}+M} \right)} \right)} = \frac{K_C \left(\frac{r_C}{\delta_C} \left(\eta + \frac{a_{MC}M}{b_{MC}+M} \right) - 1 \right)}{(b_{CM} + K_C) \frac{r_C}{\delta_C} \left(\eta + \frac{a_{MC}M}{b_{MC}+M} \right) - K_C} \\
& = \frac{K_C \left(\frac{r_C}{\delta_C} (\eta (b_{MC} + M) + a_{MC}M) - (b_{MC} + M) \right)}{(b_{CM} + K_C) \frac{r_C}{\delta_C} (\eta (b_{MC} + M) + a_{MC}M) - K_C (b_{MC} + M)} \\
& = \frac{K_C \left\{ \left[b_{MC} \left(\frac{r_C}{\delta_C} \eta - 1 \right) \right] + \left[\frac{r_C}{\delta_C} (\eta + a_{MC}) - 1 \right] M \right\}}{b_{MC} \left[(b_{CM} + K_C) \frac{r_C}{\delta_C} \eta - K_C \right] + \left[(b_{CM} + K_C) \frac{r_C}{\delta_C} (\eta + a_{MC}) - K_C \right] M} \\
& = \frac{\zeta_0 + \zeta_1 M}{\alpha_0 + \alpha_1 M}
\end{aligned}$$

with α_0 , α_1 , ζ_0 and ζ_1 defined by this relation. It follows that

$$a_{NM}\rho + (a_{CM} + a_{CNM}\rho) \frac{K_C \left(1 - \frac{1}{\frac{r_C}{\delta_C} \left(\eta + \frac{a_{MC}M}{b_{MC}+M} \right)} \right)}{b_{CM} + K_C \left(1 - \frac{1}{\frac{r_C}{\delta_C} \left(\eta + \frac{a_{MC}M}{b_{MC}+M} \right)} \right)} = \frac{\beta_0 + \beta_1 M}{\alpha_0 + \alpha_1 M} \quad (21)$$

with

$$\begin{aligned}
\alpha_0 &= b_{MC} \left[(b_{CM} + K_C) \frac{r_C}{\delta_C} \eta - K_C \right], \\
\alpha_1 &= (b_{CM} + K_C) \frac{r_C}{\delta_C} (\eta + a_{MC}) - K_C, \\
\beta_0 &= a_{NM} \rho \alpha_0 + (a_{CM} + a_{CNM} \rho) \zeta_0 \\
&= b_{MC} \left\{ a_{NM} \rho \left[(b_{CM} + K_C) \frac{r_C}{\delta_C} \eta - K_C \right] + (a_{CM} + a_{CNM} \rho) K_C \left(\frac{r_C}{\delta_C} \eta - 1 \right) \right\} \\
&= b_{MC} \left\{ a_{NM} \rho b_{CM} \frac{r_C}{\delta_C} \eta + (a_{NM} \rho + a_{CM} + a_{CNM} \rho) K_C \left(\frac{r_C}{\delta_C} \eta - 1 \right) \right\}, \\
\beta_1 &= a_{NM} \rho \alpha_1 + (a_{CM} + a_{CNM} \rho) \zeta_1 \\
&= a_{NM} \rho \left((b_{CM} + K_C) \frac{r_C}{\delta_C} (\eta + a_{MC}) - K_C \right) + (a_{CM} + a_{CNM} \rho) K_C \left[\frac{r_C}{\delta_C} (\eta + a_{MC}) - 1 \right] \\
&= a_{NM} b_{CM} \rho \frac{r_C}{\delta_C} (\eta + a_{MC}) + (a_{NM} \rho + a_{CM} + a_{CNM} \rho) K_C \left[\frac{r_C}{\delta_C} (\eta + a_{MC}) - 1 \right].
\end{aligned}$$

Author Contributions

Project initiation: Li Zhu and Helen Moore. **Project development:** all authors. **Model structure determination:** Li Zhu, Chaitali Passey, Michael Robbins, Natalie Bezman, Suresh Shelat, Hearn Jay Cho, Helen Moore. **Mathematical modeling:** Jill Gallaher, Kamila Larripa, Urszula Ledzewicz, Marissa Renardy, Blerta Shtylla, Nessy Tania, Diana White, Karen Wood, Helen Moore.

Disclosures

Li Zhu, Chaitali Passey, Michael Robbins, Natalie Bezman, Suresh Shelat, and Helen Moore were all employees of Bristol-Myers Squibb (BMS) at the time this work was done, and own stock in BMS. Urszula Ledzewicz received financial compensation from BMS for this work. Hearn Jay Cho has the following disclosures: Membership on an entity’s Board of Directors or advisory committees – BMS, Genentech Roche; Research Funding – BMS, Agenus, Inc., Genentech Roche, Janssen; Consultancy – Genentech Roche, Janssen. The other authors have no disclosures for this work.

Acknowledgements This work was initiated during the Association for Women in Mathematics collaborative workshop Women Advancing Mathematical Biology hosted by the Mathematical Biosciences Institute (MBI) at Ohio State University in April 2017. Funding for the workshop was provided by MBI, NSF ADVANCE “Career Advancement for Women Through Research-Focused Networks” (NSF-HRD 1500481), Society for Mathematical Biology, and Microsoft Research. The authors thank the anonymous reviewers for helpful comments that led to improvements in this manuscript.

References

1. Abdul K Abbas, Andrew H Lichtman, and Shiv Pillai. *Cellular and Molecular Immunology, Eighth Edition*. Elsevier Saunders, Philadelphia, PA, 2015.
2. JC Arciero, TL Jackson, and DE Kirschner. A mathematical model of tumor-immune evasion and siRNA treatment. *Discrete and Continuous Dynamical Systems Series B*, 4(1):39–58, 2004.
3. Joanna Baginska, Elodie Viry, Jérôme Paggetti, Sandrine Medves, Guy Berchem, Etienne Moussay, and Bassam Janji. The critical role of the tumor microenvironment in shaping natural killer cell-mediated anti-tumor immunity. *Frontiers in Immunology*, 4:1–13, 2013.
4. Don M Benson, Jr, Courtney E Bakan, Anjali Mishra, Craig C Hofmeister, Yvonne Efebera, Brian Becknell, Robert A Baiocchi, Jianying Zhang, Jianhua Yu, Megan K Smith, Carli N Greenfield, Pierluigi Porcu, Steven M Devine, Rinat Rotem-Yehudar, Gerard Lozanski, John C Byrd, and Michael A Caligiuri. The PD-1/PD-L1 axis modulates the natural killer cell versus multiple myeloma effect: A therapeutic target for CT-011, a novel monoclonal anti-PD-1 antibody. *Blood*, 116(13):22862294, 2010.
5. Franck Bihl, Claire Germain, Carmelo Luci, and Veronique M Braud. Mechanisms of NK cell activation: CD4+ T cells enter the scene. *Cellular and Molecular Life Sciences*, 68:3457–3467, 2011.
6. Onur Boyman and Jonathan Sprent. The role of interleukin-2 during homeostasis and activation of the immune system. *Nature Reviews Immunology*, 12(3):180, 2012.
7. Walter MT Braga, Djordje Atanackovic, and Gisele WB Colleoni. The role of regulatory T cells and TH17 cells in multiple myeloma. *Clinical and Developmental Immunology*, 2012, 2012.
8. RD Brown, B Pope, E Yuen, J Bibson, and DE Joshua. The expression of T cell related costimulatory molecules in multiple myeloma. *Leukemia & Lymphoma*, 31(3-4):379–384, 1998.
9. Ennio Carbone, Paola Neri, Maria Mesuraca, Mariateresa T Fulciniti, Takemi Otsuki, Daniela Pende, Veronika Groh, Thomas Spies, Giuditta Pollio, David Cosman, Lucio Catalano, Pierfrancesco Tassone, Bruno Rotoli, and Salvatore Venuta. HLA class I, NKG2D, and natural cytotoxicity receptors regulate multiple myeloma cell recognition by natural killer cells. *Immunobiology*, 105(1):251–258, 2005.
10. Adelheid Cerwenka, Jody Baron, and Lewis Lanier. Ectopic expression of retinoic acid early inducible-1 gene (RAE-1) permits natural killer cell-mediated rejection of a MHC class I-bearing tumor in vivo. *Proceedings of the National Academy of Sciences*, 98(20):11521–11526, 2001.
11. Mei-Ling Chen, Mikaël J Pittet, Leonid Gorelik, Richard A Flavell, Ralph Weissleder, Harald von Boehme, and Khashayarsha Khazaie. Regulatory T cells suppress tumor-specific CD8 T cell cytotoxicity through TGF- β signals in vivo. *Proceedings of the National Academy of Sciences*, 102(2):419–424, 2005.
12. Andrea K Cooper and Peter S Kim. A cellular automata and a partial differential equation model of tumor-immune dynamics and chemotaxis. In Amina Eladaddi, Peter Kim, and Dann Mallet, editors, *Mathematical Models of Tumor-Immune System Dynamics*, volume 107 of *Springer Proceedings in Mathematics and Statistics*, pages 21–46. Springer, New York, 2014.
13. Berno Dankbar, Teresa Padró, Regine Leo, Birgit Feldmann, Martin Kropff, Rolf M Mesters, Hubert Serve, Wolfgang E Berdel, and Joachim Kienast. Vascular endothelial growth factor and interleukin-6 in paracrine tumor-stromal cell interactions in multiple myeloma. *Journal of Immunology Research*, 95(8):2630–2636, 2000.
14. Giovanni D’Arena, Giovanni Rossi, Luca Laurenti, Teodora Statuto, Fiorella D’Auria, Luciana Valvano, Vittorio Simeon, Aldo Giudice, Idanna Innocenti, Vincenzo De Feo, Rosanna Filosa, and Pellegrino Musto. Circulating regulatory T-cells in monoclonal gammopathies of uncertain significance and multiple myeloma: In search of a role. *Journal of Immunology Research*, 2016:Article ID 9271469, 2016.

15. Rob J de Boer, Dirk Homann, and Alan S Perelson. Different dynamics of CD4+ and CD8+ T cell responses during and after acute lymphocytic choriomeningitis virus infection. *The Journal of Immunology*, 171(8):3928–3935, 2003.
16. Lisette de Pillis, Trevor Caldwell, Elizabeth Sarapata, and Heather Williams. Mathematical modeling of regulatory T cell effects on renal cell carcinoma treatment. *Discrete & Continuous Dynamical Systems-Series B*, 18(4), 2013.
17. Lisette de Pillis, Angela Gallegos, and Ami Radunskaya. A model of dendritic cell therapy for melanoma. *Frontiers in Oncology*, 3, 2013.
18. Lisette G de Pillis, Ami Radunskaya, and Charles L Wiseman. A validated mathematical model of cell-mediated immune response to tumor growth. *Cancer Research*, 65:7950–7958, 2005.
19. Harold P de Vladar and Jorge A González. Dynamic response of cancer under the influence of immunological activity and therapy. *Journal of Theoretical Biology*, 227(3):335–348, 2004.
20. Marcello Delitalia, Tommaso Lorenzi, and Matteo Melensi. A structured population model of competition between cancer cells and T cells under immunotherapy. In Amina Eladaddi, Peter Kim, and Dann Mallet, editors, *Mathematical Models of Tumor-Immune System Dynamics*, volume 107 of *Springer Proceedings in Mathematics and Statistics*, pages 47–58. Springer, New York, 2014.
21. Madhav V Dhodapkar, Matthew D Geller, David H Chang, Kanako Shimizu, Shin-Ichiro Fujii, Kavita M Dhodapkar, and Joseph Krasovsky. A reversible defect in natural killer T cell function characterizes the progression of premalignant to malignant multiple myeloma. *Journal of Experimental Medicine*, 197(12):1667–1676, 2003.
22. Andreas Diefenbach, Eric R Jensen, Amanda M Jamieson, and David H Raulet. Rae1 and H60 ligands of the NKG2D receptor stimulate tumor immunity. *Nature*, 413(6852):165, 2001.
23. Richard J DiPaolo, Deborah D Glass, Karen E Bijwaard, and Ethan M Shevach. CD4+ CD25+ T cells prevent the development of organ-specific autoimmune disease by inhibiting the differentiation of autoreactive effector T cells. *Journal of Immunology*, 175(11):7135–7142, 2005.
24. Alberto d’Onofrio. A general framework for modelling tumor-immune system competition and immunotherapy: Mathematical analysis and biomedical inferences. *Physica D*, 208(3-4):202–235, 2005.
25. T Dosani, M Carlsten, I Maric, and O Landgren. The cellular immune system in myeloma-genesis: NK cells and T cells in the development of MM and their uses in immunotherapies. *Blood Cancer Journal*, 5(4):e306, 2015.
26. Brian GM Durie and Sydney E Salmon. A clinical staging system for multiple myeloma: Correlation of measured myeloma cell mass with presenting clinical features, response to treatment, and survival. *Cancer*, 36:842–854, 1975.
27. Amina Eladaddi, Peter Kim, and Dann Mallet, editors. *Mathematical Models of Tumor-Immune System Dynamics*, volume 107 of *Springer Proceedings in Mathematics and Statistics*, New York, 2014. Springer.
28. James Favaloro, Ross Brown, Esther Aklilu, Shihong Yang, Hayley Suen, Derek Hart, Phillip Fromm, John Gibson, Liane Khoo, P Joy Ho, and Douglas Joshua. Myeloma skews regulatory T and pro-inflammatory T helper 17 cell balance in favor of a suppressive state. *Leukemia & Lymphoma*, 55(5):10901098, 2014.
29. Sylvia Feyler, Gina B Scott, Christopher Parrish, Sarah Jarmin, Paul Evans, Mike Short, Katherine McKinley, Peter J Selby, and Gordon Cook. Tumour cell generation of inducible regulatory T-cells in multiple myeloma is contact-dependent and antigen-presenting cell-independent. *PLoS ONE*, 7(5):e35981, 2012.
30. Sylvia Feyler, Marie von Lilienfeld-Toal, Sarah Jarmin, Lee Marles, Andy Rawstron, AJ Ashcroft, Roger G Owen, Peter J Selby, and Gordon Cook. CD4+CD25+FoxP3+ regulatory T cells are increased whilst CD3+CD4CD8abTCR+ double negative T cells are decreased in the peripheral blood of patients with multiple myeloma which correlates with disease burden. *British Journal of Haematology*, 144:686695, 2009.
31. Federico Frascoli, Peter S Kim, Barry D Hughes, and Kerry A Landman. A dynamical model of tumour immunotherapy. *Mathematical Biosciences*, 253:50–62, 2014.

32. Christoph Frohn, Maike Hoppner, Peter Schlenke, Holger Kirchner, Petra Koritke, and Jurgen Luhm. Anti-myeloma activity of natural killer lymphocytes. *British Journal of Haematology*, 119:660–664, 2002.
33. Dmitry I Gabrilovich, Hailei L Chen, Khaled R Girgis, H Thomas Cunningham, GERALYN M Meny, Sorena Nadaf, Denise Kavanaugh, and David P Carbone. Production of vascular endothelial growth factor by human tumors inhibits the functional maturation of dendritic cells. *Nature Medicine*, 2(10):1096–1103, 1996.
34. Minjie Gao, Lu Gao, Guang Yang, Yi Tao, Jun Hou, Hongwei Xu, Xiaojing Hu, Ying Han, Qianqiao Zhang, Fenghuang Zhan, Xiaosong Wu, and Jumei Shi. Myeloma cells resistance to NK cell lysis mainly involves an HLA class I-dependent mechanism. *Acta Biochimica et Biophysica Sinica*, 46(7):597–604, 2014.
35. François Ghiringhelli, Cédric Ménard, Francois Martin, and Laurence Zitvogel. The role of regulatory T cells in the control of natural killer cells: Relevance during tumor progression. *Immunological Reviews*, 214(1):229–238, 2006.
36. François Ghiringhelli, Cédric Ménard, Magali Terme, Caroline Flament, Julien Taieb, Nathalie Chaput, Pierre E Puig, Sophie Novault, Bernard Escudier, Eric Vivier, et al. CD4+ CD25+ regulatory T cells inhibit natural killer cell functions in a transforming growth factor- β -dependent manner. *Journal of Experimental Medicine*, 202(8):1075–1085, 2005.
37. Güllü Görgün, Mehmet K Samur, Kristen B Cowens, Steven Paula, Giada Bianchi, Julie E Anderson, Randie E White, Ahaana Singh, Hiroto Ohguchi, Rikio Suzuki, Shohei Kikuchi, Takeshi Harada, Teru Hideshima, Yu-Tzu Tai, Jacob P Laubach, Noopur Raje, Florence Margeas, Stephane Minvielle, Herve Avet-Loiseau, Nikhil C Munshi, David M Dorfman, Paul G Richardson, and Kenneth C Anderson. Lenalidomide enhances immune checkpoint blockade-induced immune response in multiple myeloma. *Clinical Cancer Research*, 21(20):4607–4618, 2015.
38. Charlotte T Hansen, Per T Pedersen, Lars C Nielsen, and Niels Abildgaard. Evaluation of the serum free light chain (sFLC) analysis in prediction of response in symptomatic multiple myeloma patients: Rapid profound reduction in involved FLC predicts achievement of VGPR. *European Journal of Haematology*, 93(5):407–413, 2014.
39. Charles A Janeway. How the immune system protects the host from infection. *Microbes and Infection*, 3(13):1167–1171, 2001.
40. F Jonsson, Y Ou, L Claret, D Siegel, S Jagannath, R Vij, A Badros, S Aggarwal, and R Bruno. A tumor growth inhibition model based on M-protein levels in subjects with relapsed/refractory multiple myeloma following single-agent carfilzomib use. *CPT: Pharmacometrics & Systems Pharmacology*, 4(12):711–719, 2015.
41. Yawara Kawano, Michele Moschetta, Salomon Manier, Siobhan Glavey, Güllü T Görgün, Aldo M Roccaro, Kenneth C Anderson, and Irene M Ghobrial. Targeting the bone marrow microenvironment in multiple myeloma. *Immunological Reviews*, 263(1):160–172, 2015.
42. You Kwarada, Ruth Ganss, Natalio Garbi, Torsten Sacher, Bernd Arnold, and Günter J Hämmerling. NK-and CD8+ T cell-mediated eradication of established tumors by peritumoral injection of CpG-containing oligodeoxynucleotides. *The Journal of Immunology*, 167(9):5247–5253, 2001.
43. Dickran Kazandjian and Ola Landgren. A look backward and forward in the regulatory and treatment history of multiple myeloma: Approval of novel-novel agents, new drug development, and longer patient survival. *Seminars in Oncology*, 43:682689, 2016.
44. Jeong M Kim, Jeffrey P Rasmussen, and Alexander Y Rudensky. Regulatory T cells prevent catastrophic autoimmunity throughout the lifespan of mice. *Nature Immunology*, 8(2):191, 2007.
45. Denise Kirschner and John Carl Panetta. Modeling immunotherapy of the tumor-immune interaction. *Journal of Mathematical Biology*, 37:235–252, 2007.
46. Mehmet Kocoglu and Ashraf Badros. The role of immunotherapy in multiple myeloma. *Pharmaceuticals (Basel)*, 9(1):3, 2016.
47. Jakub Krejčík, Tineke Casneuf, Inger S Nijhof, Bie Verbist, Jaime Bald, Torben Plesner, Khaja Syed, Kevin Liu, Niels WCJ van de Donk, Brendan M Weiss, Tahamtan Ahmadi, Henk M

- Lokhorst, Tuna Mutis, and A Kate Sasser. Daratumumab depletes CD38+ immune regulatory cells, promotes T-cell expansion, and skews T-cell repertoire in multiple myeloma. *Blood*, 128(3):384–394, 2016.
48. Vladimir A Kuznetsov, Iliya A Makalkin, Mark A Taylor, and Alan S Perelson. Nonlinear dynamics of immunogenic tumors: Parameter estimation and global bifurcation analysis. *Bulletin of Mathematical Biology*, 56(2):295–321, 1994.
 49. RA Kyle, ED Remstein, TM Therneau, A Dispenzieri, PJ Kurtin, JM Hodnefield, DR Larson, MF Plevak, DF Jelinek, R Fonseca, LJ Melton 3rd, and SV Rajkumar. Clinical course and prognosis of smoldering (asymptomatic) multiple myeloma. *New England Journal of Medicine*, 356(25):2582–2590, 2007.
 50. RA Kyle, TM Therneau, SV Rajkumar, JR Offord, DR Larson, MF Plevak, and LJ Melton 3rd. A long-term study of prognosis in monoclonal gammopathy of undetermined significance. *New England Journal of Medicine*, 346(8):564–569, 2002.
 51. Robert A Kyle, Morie A Gertz, Thomas E Witzig, John A Lust, Martha Q Lacy, Angela Dispenzieri, Rafael Fonseca, S Vincent Rajkumar, Janice R Offord, Dirk R Larson, Matthew E Plevak, Terry M Therneau, and Philip R Greipp. Review of 1027 patients with newly diagnosed multiple myeloma. *Mayo Clinic Proceedings*, 78:21–33, 2003.
 52. Urszula Ledzewicz and Helen Moore. Dynamical systems properties of a mathematical model for the treatment of CML. *Applied Sciences*, 6(291), 2016.
 53. Urszula Ledzewicz, Mohhammad Naghnaeian, and Heinz Schättler. Optimal response to chemotherapy for a mathematical model of tumor-immune dynamics. *Journal of Mathematical Biology*, 64:557–577, 2012.
 54. Christof Lehman, Matthias Zeis, and Lutz Uharek. Activation of natural killer cells with interleukin 2 (IL-2) and IL-12 increases perforin binding and subsequent lysis of tumour cells. *British Journal of Haematology*, 114(3):660–665, 2001.
 55. Kang-Ling Liao, Xue-Feng Bai, and Avner Friedman. Mathematical modeling of interleukin-27 induction of anti-tumor T cells response. *PLoS ONE*, 9(3):e91844, 2014.
 56. Alice Maniatis. Pathophysiology of paraprotein production. *Renal Failure*, 20(6):821–828, 1998.
 57. Thorsten R Mempel, Mikael J Pittet, Khashayarsha Khazaie, Wolfgang Weninger, Ralph Weissleder, Harald von Boehmer, and Ulrich H von Andrian. Regulatory T cells reversibly suppress cytotoxic T cell function independent of effector differentiation. *Immunity*, 25(1):129–141, 2006.
 58. Neal J Meropol, Grace M Barresi, Todd A Fehniger, James Hitt, Margaret Franklin, and Michael A Caligiuri. Evaluation of natural killer cell expansion and activation in vivo with daily subcutaneous low-dose interleukin-2 plus periodic intermediate-dose pulsing. *Cancer Immunology and Immunotherapy*, 46(6):318–326, 1998.
 59. Adriana J Michielsen, Andrew E Hogan, Joseph Marry, Miriam Tosetto, Fionnuala Cox, John M Hyland, Kieran D Sheahan, Diarmuid P O’Donoghue, Hugh E Mulcahy, Elizabeth J Ryan, and Jacintha N O’Sullivan. Tumour tissue microenvironment can inhibit dendritic cell maturation in colorectal cancer. *PLoS ONE*, 6(11):e27944, 2011.
 60. JR Mills, DR Barnidge, A Dispenzieri, and DL Murray. High sensitivity blood-based M-protein detection in sCR patients with multiple myeloma. *Blood Cancer Journal*, 7(8):e590, 2017.
 61. Helen Moore and Natasha K Li. A mathematical model for chronic myelogenous leukemia (CML) and T cell interaction. *Journal of Theoretical Biology*, 227(4):513–523, 2004.
 62. Seema Nanda, Helen Moore, and Suzanne Lenhart. Optimal control of treatment in a mathematical model of chronic myelogenous leukemia. *Mathematical Biosciences*, 210(1):143–156, 2007.
 63. Theodore X O’Connell, Timothy J Horita, and Barsam Kasravi. Understanding and interpreting serum protein electrophoresis. *American Family Physician*, 71(1):105–112, 2005.
 64. Tiina M Oivanen. Plateau phase in multiple myeloma: An analysis of long-term follow-up of 432 patients. *British Journal of Haematology*, 92(4):834–839, 1996.
 65. Katharina Pallmer and Annette Oxenius. Recognition and regulation of T cells by NK cells. *Frontiers in Immunology*, 7, 2016.

66. Drew M Pardoll. The blockade of immune checkpoints in cancer immunotherapy. *Nature Reviews Cancer*, 12:252–264, 2012.
67. Tatiana Pazina, Ashley M James, Alexander W MacFarlane IV, Natalie A Bezman, Karla A Henning, Christine Bee, Robert F Graziano, Michael D Robbins, Adam D Cohen, and Kerry S Campbell. The anti-SLAMF7 antibody elotuzumab mediates NK cell activation through both CD16-dependent and independent mechanisms. *Oncot Immunology*, 6(9), 2017.
68. Roberto J. Pessoa de Magalhães, María-Belén Vidriales, Bruno Paiva, Carlos Fernandez-Gimenez, Ramón García-Sanz, María-Victoria Mateos, Norma C. Gutierrez, Quentin Lecrevisse, Juan F Blanco, Jose Hernández, Natalia de las Heras, Joaquin Martinez-Lopez, Monica Roig, Elaine Sobral Costa, Enrique M. Ocio, Martin Perez-Andres, Angelo Maiolino, Marcio Nucci, Javier De La Rubia, Juan-Jose Lahuerta, Jesús F. San-Miguel, and Alberto Orfao. Analysis of the immune system of multiple myeloma patients achieving long-term disease control by multidimensional flow cytometry. *Haematologica*, 98(1):79–86, 2013.
69. Guy Pratt, Oliver Goodyear, and Paul Moss. Immunodeficiency and immunotherapy in multiple myeloma. *British Journal of Haematology*, 138:563–579, 2007.
70. M Raitakari, RD Brown, J Gibson, and DE Joshua. T cells in myeloma. *Hematological Oncology*, 21(1):33–42, 2003.
71. Karthick Raja Muthu Raja, Lucie Rihova, Lenka Zahradova, Maria Klincova, Miroslav Penka, and Roman Hajek. Increased T regulatory cells are associated with adverse clinical features and predict progression in multiple myeloma. *PLoS ONE*, 7(10):e47077, 2012.
72. Marina Ratta, Francesco Fagnoni, Antonio Curti, Rosanna Vescovini, Paolo Sansoni, Barbara Oliviero, Miriam Fogli, Elisa Ferri, Gioacchino Robustelli Della Cuna, Sante Tura, Michele Baccarani, and Roberto M Lemoli. Dendritic cells are functionally defective in multiple myeloma: The role of interleukin-6. *Blood*, 100(1):230–237, 2002.
73. Mark Robertson-Tessi, Ardith El-Kareh, and Alain Goriely. A mathematical model of tumor-immune interactions. *Journal of Theoretical Biology*, 294:56–73, 2012.
74. Sydney E Salmon and Beth A Smith. Immunoglobulin synthesis and total body tumor cell number in IgG multiple myeloma. *Journal of Clinical Investigation*, 49:1114–1121, 1970.
75. Heinz Schättler and Urszula Ledzewicz. *Optimal Control for Mathematical Models of Cancer Therapies*. Springer, New York, 2015.
76. Anil Shanker, Michel Buferne, and Anne-Marie Schmitt-Verhulst. Cooperative action of CD8 T lymphocytes and natural killer cells controls tumour growth under conditions of restricted T-cell receptor diversity. *Immunology*, 129(1):41–54, 2010.
77. Anil Shanker, Grgory Verdeil, Michel Buferne, Else-Marit Inderberg-Suso, Denis Puthier, Florence Joly, Catherine Nguyen, Lee Leserman, Nathalie Auphan-Anezin, and Anne-Marie Schmitt-Verhulst. CD8 T cell help for innate antitumor immunity. *Journal of Immunology*, 179(10):6651–6662, 2007.
78. Ethan M Shevach, Richard A DiPaolo, John Andersson, Dong-Mei Zhao, Geoffrey L Stephens, and Angela M Thornton. The lifestyle of naturally occurring CD4+ CD25+ Foxp3+ regulatory T cells. *Immunological Reviews*, 212(1):60–73, 2006.
79. David R Shook and Dario Campana. Natural killer cell engineering for cellular therapy of cancer. *Tissue Antigens*, 78(6):409–415, 2011.
80. Rebecca L Siegel, Kimberly D Miller, and Ahmedin Jemal. Cancer statistics, 2016. *CA: A Cancer Journal for Clinicians*, 66:7–30, 2016.
81. Mark J Smyth, Michele WL Teng, Jeremy Swann, Konstantinos Kyparissoudis, Dale I Godfrey, and Yoshihiro Hayakawa. CD4+ CD25+ T regulatory cells suppress NK cell-mediated immunotherapy of cancer. *Journal of Immunology*, 176(3):1582–1587, 2006.
82. Dorothy K Sojka, Yu-Hui Huang, and Deborah J Fowell. Mechanisms of regulatory T-cell suppression a diverse arsenal for a moving target. *Immunology*, 124(1):13–22, 2008.
83. Eduardo D Sontag. A dynamic model of immune responses to antigen presentation predicts different regions of tumor or pathogen elimination. *Cell Systems*, 4(2):231–241, 2017.
84. NV Stepanova. Course of the immune reaction during the development of a malignant tumour. *Biophysics*, 24:917–923, 1980.

85. H Suen, R Brown, S Yang, C Weatherburn, PJ Ho, N Woodland, N Nassif, P Barbaro, C Bryant, D Hart, J Gibson, and D Joshua. Multiple myeloma causes clonal T-cell immunosenescence: Identification of potential novel targets for promoting tumour immunity and implications for checkpoint blockade. *Leukemia*, 30(8):1716–1724, 2016.
86. Peter W Sullivan and Sydney E Salmon. Kinetics of tumor growth and regression in IgG multiple myeloma. *Journal of Clinical Investigation*, 51:1697–1708, 1972.
87. Can M Sungur, Yajarayma J Tang-Feldman, Erik Ames, Maite Alvarez, Mingyi Chen, Dan L Longo, Claire Pomeroy, and William J Murphy. Murine natural killer cell licensing and regulation by T regulatory cells in viral responses. *Proceedings of the National Academy of Sciences*, 110(18):7401–7406, 2013.
88. George W Swan and Thomas L Vincent. Optimal control analysis in the chemotherapy of IgG multiple myeloma. *Bulletin of Mathematical Biology*, 39(3):317–337, 1977.
89. Min Tang, Rui Zhao, Helgi van de Velde, Jennifer G Tross, Constantine Mitsiades, Suzanne Viselli, Rachel Neuwirth, Dixie-Lee Esseltine, Kenneth Anderson, Irene M Ghobrial, Jesús F San Miguel, Paul G Richardson, Michael H Tomasson, and Franziska Michor. Myeloma cell dynamics in response to treatment supports a model of hierarchical differentiation and clonal evolution. *Clinical Cancer Research*, 22(16):4206–4214, 2016.
90. Dat Q Tran. TGF- β : The sword, the wand, and the shield of FOXP3+ regulatory T cells. *Journal of Molecular Cell Biology*, 4(1):29–37, 2012.
91. Trisilowati, Scott W McCue, and Dann G Mallet. A cellular automata model to investigate immune cell-tumor cell interactions in growing tumors in two spatial dimensions. In Amina Eladaddi, Peter Kim, and Dann Mallet, editors, *Mathematical Models of Tumor-Immune System Dynamics*, volume 107 of *Springer Proceedings in Mathematics and Statistics*, pages 223–251. Springer, New York, 2014.
92. Milica Vukmanovic-Stejic, Yan Zhang, Joanne E Cook, Jean M Fletcher, Arthur McQuaid, Joanne E Masters, Malcolm HA Rustin, Leonie S Taams, Peter CL Beverley, Derek C Macallan, et al. Human CD4+ CD25hi Foxp3+ regulatory T cells are derived by rapid turnover of memory populations in vivo. *Journal of Clinical Investigation*, 116(9):2423, 2006.
93. Hillary S Warren. NK cell proliferation and inflammation. *Immunology and Cell Biology*, 74:473–480, 1996.
94. Yue-Jin Wen, Bart Barlogie, and Qing Yi. Idiotype-specific cytotoxic t lymphocytes in multiple myeloma: Evidence for their capacity to lyse autologous primary tumor cells. *Blood*, 97(6):1750–1755, 2001.
95. Yue-Jin Wen, Rui Min, Guido Tricot, Bart Barlogie, and Qing Yi. Tumor lysate-specific cytotoxic T lymphocytes in multiple myeloma: Promising effector cells for immunotherapy. *Blood*, 99(9):3280–3285, 2002.
96. Yan Zhang, Diana L Wallace, Catherine M De Lara, Hala Ghattas, Becca Asquith, Andrew Worth, George E Griffin, Graham P Taylor, David F Tough, Peter CL Beverley, et al. In vivo kinetics of human natural killer cells: The effects of ageing and acute and chronic viral infection. *Immunology*, 121(2):258–265, 2007.